Occurrence, abundance, and formation of atmospheric tarballs from a wide range of wildfires in the western US

Kouji Adachi[1], Jack E. Dibb[2], Joseph M. Katich[3,4#], Joshua P. Schwarz[3], Hongyu Guo[4,5], Pedro Campuzano-Jost[4,5], Jose L. Jimenez[4,5], Jeff Peischl[3], Christopher D. Holmes[6], James Crawford[7]

[1]Department of Atmosphere, Ocean, and Earth System Modelling Research, Meteorological Research Institute, Tsukuba, Japan
[2]Institute for the Study of Earth, Oceans, and Space, University of New Hampshire, Durham, NH, USA
[3]Chemical Sciences Laboratory, National Oceanic and Atmospheric Administration, Boulder, CO, USA
[4]Cooperative Institute for Research in Environmental Sciences, University of Colorado Boulder, Boulder, CO, USA
[5]Department of Chemistry, University of Colorado Boulder, Boulder, CO, USA
[6]Earth, Ocean, and Atmospheric Science, Florida State University, Tallahassee, FL, USA
[7]NASA Langley Research Center, Hampton, VA, USA
[#]now at Ball Aerospace, Boulder, CO, USA

Correspondence to: Kouji Adachi (adachik@mri-jma.go.jp)

Abstract. Biomass burning emits large numbers of organic aerosol particles, a subset of which are called tarballs (TBs). TBs possess spherical morphology and unique physical, chemical, and optical properties. They are recognized as brown carbon aerosol particles, thereby having implications for climate through the absorption of solar radiation. Aerosol particles were collected from wildfire and agricultural fire smoke sampled by the NASA DC-8 aircraft during the FIREX-AQ campaign in the western US from July to September 2019. The current study developed an image analysis method applying deep learning to distinguish TBs from other round particles that deformed on the substrate, based on their morphological characteristics in the transmission electron microscopy images. This study detected 4567 TBs with most <10 h downwind from the emissions and measured their compositions, abundance, sizes, and mixing states. The number fraction, mass fraction, and concentration of TBs from all wildfire smoke were 10% ± 1%, 10% ± 2%, and 10.1 ± 4.6 µg m^{-3}, respectively. As the smoke aged from emission up to 5 h, the TB number fractions roughly increased from 5% to 15%, indicating that TBs are processed primary particles. We also showed TBs within pyrocumulonimbus (PyroCb) activity and various TB mixing states. This study reveals the abundances and physical and chemical properties of a wide range of TBs from various biomass-burning events and enhances the knowledge of TB emissions, which contributes to the evaluation of the climate impact of TBs.

1 Introduction

Open biomass burning (e.g., wildfire, agricultural fire) emits significant amounts of gases and particulate matter into the atmosphere (Yokelson et al., 2007; Andreae, 2019; Gkatzelis et al., 2024) and largely influences the global climate (Szopa et al., 2021) and human health (Karanasiou et al., 2021). While the future impacts of biomass burning are highly uncertain, a warmer climate will likely increase fire frequency and severity (Keywood et al., 2011; Abatzoglou and Williams, 2016; Jaffe et al., 2020), implying that they will significantly influence the future climate.

The influences of biomass burning on the climate include both cooling and warming effects. The emissions of light-scattering aerosol particles generally have a negative influence on the radiative forcing. In contrast, the emissions of greenhouse gases and light-absorbing aerosol particles enhance the positive radiative forcing (Szopa et al., 2021). As a result of both negative and positive effects, the overall climate effect of biomass burning is subject to a large degree of uncertainty (Szopa et al., 2021).

Brown carbon is a type of organic aerosol particle commonly emitted from biomass burning. It is characterized by an absorption spectrum that smoothly increases from visible to ultraviolet wavelengths (Laskin et al., 2015). Because of their light-absorbing properties, they have positive radiative forcing effects (Andreae and Gelencsér, 2006; Laskin et al., 2015). Brown carbon aerosol particles from biomass burning have various compositions, volatilities, optical properties, and formation processes, and this study focuses on a specific type of brown carbon aerosol particles called tarball (TB).

TBs were first recognized and defined in companion papers by Li et al. (2003) and Pósfai et al. (2003) from biomass burning aerosol samples in southern Africa using transmission electron microscopy (TEM). Pioneering studies have revealed their detailed chemical and physical properties (Pósfai et al., 2004; Hand et al., 2005). Since then, TBs have been reported in various locations across the globe, including biomass burning smoke (e.g., Adachi and Buseck, 2011; Adachi et al., 2019), urban areas (e.g., Fu et al., 2012; Sparks and Wagner, 2021), remote mountains (e.g., Yuan et al., 2020), the oceanic atmosphere (e.g., Yoshizue et al., 2020), and the Arctic region (e.g., Moroni et al., 2017; Moroni et al., 2020; Adachi et al., 2021).

TBs are commonly defined based on their unique physical properties, such as spherical shapes and insensitivity to electron beams and heat (Pósfai et al., 2004; Hand et al., 2005; Chakrabarty et al., 2010; China et al., 2013; Adachi et al., 2017; Corbin and Gysel-Beer, 2019). Further TB measurements have also revealed that they have light-absorbing optical properties (Hand et al., 2005; Chakrabarty et al., 2010; Sedlacek, et al., 2018; Mathai et al., 2023). Thus, it is hypothesized that they have notable climate influences because of their light-absorbing properties and abundance of biomass burning emissions (Jacobson, 2012; Chakrabarty et al., 2023). In addition, studies suggest that TBs possibly act as ice-nucleating particles (INPs) (Barry et al., 2021) and adversely affect human health (Pardo et al., 2020). Despite their potential influences on various environmental aspects, their atmospheric abundance, formation processes, and influences on climate and human health are not fully understood and remain uncertain. A reason for this uncertainty is the difficulty of TB detection. Corbin and Gysel-Beer (2019) demonstrated that TBs can be detected using an online measurement (single particle soot photometer). However, most studies manually identify TBs by observing their spherical shapes one by one in samples collected on a filter substrate using microscopic techniques such as electron microscopy and synchrotron-based X-ray microspectroscopy (Tivanski et al., 2007; China et al., 2013).

The optical properties of TBs are of great interest in evaluating their climate influences. Previous studies have shown that TBs have a wide range of light-absorbing properties (Hand et al., 2005; Alexander et al., 2008; Chakrabarty et al., 2010; Tóth et al., 2014; Hoffer et al., 2016; Sedlacek et al., 2018; Chakrabarty et al., 2023). Although the current study does not aim to evaluate their optical properties directly, Chakrabarty et al. (2023) have shown a range of TB refractive indices across wavelengths from 350 to 1200 nm in samples collected on the ground during the current study.

The formation process of TBs is controversial. Thermal, chemical, and physical processes, such as polymerization of organic matter, condensation, photochemical processes, water loss, heat shock, and temperature changes, have been proposed to contribute to the TB formation (Pósfai et al., 2004; Laskin et al., 2015; Reid et al., 2018; Corbin and Gysel-Beer,

2019; Adachi et al., 2019). Laboratory experiments have also shown that TBs are produced by the direct emission of liquid tar droplets followed by heat transformation (Tóth et al., 2014). An aircraft-based sampling of biomass burning smoke and TEM measurements observed gradual processes forming TBs or an organic viscosity increment within biomass burning smoke (Pósfai et al., 2004; Adachi and Buseck, 2011; Sedlacek et al., 2018; Adachi et al., 2019). A previous study (Adachi et al., 2019) proposed that chemical processes involving oxygen and nitrogen addition could contribute to TB formation or occur together with the TB formation. They suggested that more observations are necessary to support the hypothesized processes.

We collected biomass burning smoke samples during the NOAA/NASA Fire Influence on Regional to Global Environments and Air Quality (FIREX-AQ) campaign (Warneke et al., 2023). The FIREX-AQ campaign explored aerosol and gas emissions from wildfires and agricultural fires using aircraft, satellite remote sensing, modeling, and ground-based measurements over the western and southeastern US during the summer of 2019. Results from the FIREX-AQ campaign include observations of the physical, chemical, and optical properties of aerosol particles (Junghenn Noyes et al., 2020; Moore et al., 2021; Sumlin et al., 2021; Adachi et al., 2022a; Zeng et al., 2022; Chakrabarty et al., 2023; Katich et al., 2023; Pagonis et al., 2023; Siemens et al., 2024; Beeler et al., 2024), ozone chemistry (Xu et al., 2021), evolution of volatile organic compounds (Decker et al., 2021; Liao et al., 2021), and emission factors (Travis et al., 2023; Gkatzelis et al. 2024) from biomass burning emissions.

Our previous study using the TEM samples from the FIREX-AQ campaign showed that ash-bearing particles characterized by Mg and Ca were abundant in fine particles (Adachi et al., 2022a). The current study used the same set of TEM samples and analyzed the data, focusing on TBs by developing an image analysis method to automatically detect TBs. The objectives of this study are to 1) develop a TB detection method from TEM images, 2) provide atmospheric observations of TBs collected from a wide range of wildfires and aging, and 3) discuss TB occurrences, including mixing states, abundances, mass concentrations, formation processes, and cloud interactions to evaluate their overall potential climate influences.

2 Methods

2.1 The FIREX-AQ campaign

The FIREX-AQ campaign was conducted from 24 July to 16 August based in Boise, Idaho, to measure wildfire and from 19 August to 3 September based in Salina, Kansas, to measure prescribed and agricultural fire (Table 1). This campaign used four aircraft, four mobile laboratories, and six ground observatories (Warneke et al., 2023). We used samples collected from the NASA DC8. The DC8 is an aircraft with various instruments and conducted a total of 20 flights during the campaign. We analyzed 221 TEM grids (53,727 particles) from nine flights that included relatively intense wildfire events and agricultural fires (Adachi et al., 2022a).

Table 1. TEM samples and detected TB information for wildfire and agricultural fire measured in this study.

Date	Main fires	State	Latitude	Longitude	TEM sample #	Particle #	TB #	TB number fractions (%)[a]	Final burned area (acres)[b]	Primary fuels[b,c]
25-Jul	Shady	ID	44.52	115.02	22	6130	619	10±3	6,091	Timber litter and shrubs under Douglas-fir, Pacific ponderosa-lodgepole pine/oceanspray forest
06-Aug	Horsefly	MT	46.96	112.44	24	6317	818	13±4	1,352	Subalpine fir-lodgepole pine-whitebark pine-Engelmann spruce forest
07-Aug	Williams Flats	WA	47.94	118.62	24	5873	80	1±1	44,360	Ignited in primarily Idaho fescue-bluebunch wheatgrass grassland and expanded to primarily Douglas-fir-Pacific ponderosa pine/oceanspray forest
08-Aug					21	5430	163	3±1		
12-Aug	Castle	AZ	36.53	112.23	24	6062	761	13±3	19,378	Ponderosa pine-two-needle pinyon-Utah juniper forest
13-Aug					24	5660	1112	20±4		
15-Aug	Sheridan	AZ	34.68	112.89	22	5139	451	9±2	21,483	Pinyon-Utah juniper forest
16-Aug					24	5801	505	9±2		
03-Sep	Agricultural biomass burning[d]	IL, MO, AR, MS	33.5-37.5	88.6-91.7	36	7315	58	1±1		Crop residue (rice and corn)
Total					221	53727	4567	9±1		

a: Uncertainty ranges are 95% confidence intervals.

b: Warneke et al. (2023)

c: Fuel characteristic classification system (FCCS) name except the agricultural biomass burning (3-Sep)

d: Agricultural biomass burning samples were collected from various occurrences of smoke in the region.

2.2 Smoke age estimate

The smoke age during the sampling of the TEM samples was estimated from air parcel trajectories computed in the HYSPLIT (Hybrid Single-Particle Lagrangian Integrated Trajectory) model (Stein et al., 2015) with multiple high-resolution meteorological datasets (HRRR 3 km, NAM CONUS Nest 3 km, and GFS 0.25°). Typical uncertainties in the smoke age originate from, for example, the difference between observed and archived wind speed data and are 25% of the estimated age (Decker et al., 2021). Other studies have also provided details of the smoke age estimates during the FIREX-AQ campaign (Xu et al., 2021; Decker et al., 2021; Zeng et al., 2022; Warneke et al., 2023).

2.3 TEM sample collection

We collected smoke and background (non-smoke) aerosol particle samples using an impactor sampler (AS-24W, Arios Inc., Tokyo, Japan) (Adachi et al., 2022b; Adachi et al., 2023), which was equipped with two TEM grids containing overlapping Lacy carbon (top; U1001, EM-Japan, Tokyo, Japan) and Formvar substrates (bottom; U1007, EM-Japan, Tokyo, Japan). This study primarily used the Formvar substrates to observe TB shapes with a flat background image. The collected particles have small and large 50% cutoff sizes of aerodynamic diameters of 100 and 700 nm, respectively. We used a common aerosol inlet operated by the NASA Langley Aerosol Research Group (LARGE) on the DC-8 (McNaughton et al., 2007; Moore et al., 2021; Brock et al., 2019). The upper cutoff aerodynamic diameter for 50% passing efficiency of aerosol particles by the inlet depends on aircraft speed and particle density (McNaughton et al., 2007), but is much larger than that of the TEM sampler, resulting in minimal effect on the TEM samples. Sampling was performed to cover each transect of biomass burning smoke, with sampling times of ~1 to 3 min and an airflow rate of 1.0 L/min.

2.4 TEM analysis

A transmission electron microscope (JEM-1400, JEOL, Tokyo, Japan) equipped with an energy-dispersive X-ray spectrometer (EDS; X-Max 80, Oxford Instruments, Tokyo, Japan) was used in the TEM and scanning TEM (STEM-EDS) modes. The STEM-EDS measurements were performed using an acceleration voltage of 120 keV and an acquisition time of 20 s. Approximately 30 TEM images were initially taken across the sample grid to measure the particle shapes and select the representative areas. Then, the areas of approximately 100 representative particles were measured in the STEM mode at a

magnification of ×6000. Appropriate thresholds were applied to dark-field STEM images to identify and distinguish aerosol particles from the substrate (Adachi et al., 2019). The smallest particle cutoff size for STEM-EDS analysis was 250 nm in area-equivalent diameter (number of pixels > 100). Characteristics of particles, such as area-equivalent diameter, shape factor, and EDS spectra, were determined from the measured particles. Area-equivalent diameters of TBs can be approximated to the volume-equivalent diameters as they retain spherical shapes. However, when the collected particles deform or spread on the substrate, the area-equivalent diameter tends to be approximately twice the volume-equivalent diameter (Zhang et al., 2020). These assumptions were applied to estimate the particle volumes.

The TEM analysis will include possible changes in particle shape after sampling. Volatile and semi-volatile particles may be lost during sampling and in the vacuum TEM chamber, causing a shape deformation of such materials. The particle height on the substrate may decrease post-collection due to the loss of volatile materials, but the base will remain the same area due to the friction and adhesion forces and will retain its original area-equivalent diameter. An increase in relative humidity after sampling will change the particle shapes and could increase the apparent aerodynamic diameter (Cheng et al., 2021). Thus, we kept the samples dry during the campaign with a desiccant and stored them in a desiccator after the campaign. Comparison of early TEM images with STEM-EDS performed up to a year later suggest that the samples were stable in storage over the time period of post-collection analysis.

The STEM-EDS provided relative weight percentages among the selected elements (C, N, O, Na, Mg, Al, Si, P, S, Cl, K, Ca, Ti, Mn, Fe, and Zn) within each particle. EDS signals of C and O can also originate from the carbon substrate. The influence of the substrate is large when measuring thin organic coatings, and their EDS intensities from the substrate can be up to half that of the organics (Adachi et al. 2016). However, thick carbonaceous particles, such as TBs and soot particles, have C signals ~7 times higher than the substrate (Adachi et al., 2016), making them clearly distinguishable from the substrate. We estimated the possible N and O wt% within TBs and other organic (carbonaceous) particles originating only from their organic compounds. This calculation was done by assuming that all sulfur forms ammonium and potassium sulfates and that any leftover N and O other than sulfate were associated with organic matter (called "non-sulfate" N and O), i.e., we assumed that all Cl, K, S, N, and O in aerosol particles occur as follows: $[Cl] = KCl$; $[K] = KCl + K_2SO_4$; $[S] = K_2SO_4 + (NH_4)_2SO_4$; $[N] = (NH_4)_2SO_4 + [N$ in non-sulfate$]$; $[O] = [O$ in non-sulfate$] + [O$ in $K_2SO_4 + (NH_4)_2SO_4]$. Further discussion of this calculation and uncertainties have been provided by Adachi et al. (2019). The previous study used normalized O/K and N/K values to avoid the influence of uneven lacey carbon substrates. In the current study, we used the O and N values directly without normalizing them by K because we used flat formvar substrates, and the influence of C and O from the substrate did not significantly influence the measured wt% of other elements. The uncertainty for light elements (N and O) was generally high and was evaluated as 5% or less (Adachi et al., 2019). Detection limits were typically 0.02 wt%, derived from one sigma of the measured peak intensities. Adachi et al. (2022a) also described details of the TEM measurements.

2.5 Tarball detection using image analysis with deep learning and particle classification

Tarballs are generally identified by their spherical shape in TEM images. However, when using a flat formvar substrate, other low-viscosity organic particles can also appear round in the TEM image as they spread uniformly over the substrates. Here, we use the contrast of TBs in TEM images differing from that of spreading organic particles, i.e., TB particles are thicker and darker than the spreading organic particles due to their sphericity on the substrate (Fig.1). We used deep learning image analysis software (MIPAR™ version 3.3.4) to identify TBs based on their morphological and imaging features (e.g., round and dark) in TEM images. Such deep learning image analysis can be achieved by first preparing training images (manually identified TB images) and then training the TEM model using the training images. After building the model, we applied it to all TEM images used for STEM-EDS analysis. The advantages of deep learning image analysis over the conventional technique are 1) it can detect TB much quicker than the conventional technique (i.e., ~ seconds vs. minutes for a

TEM image) and 2) it does not depend on the experience of the operator, whereas the conventional method needs substantial training and experience to unambiguously identify TBs.
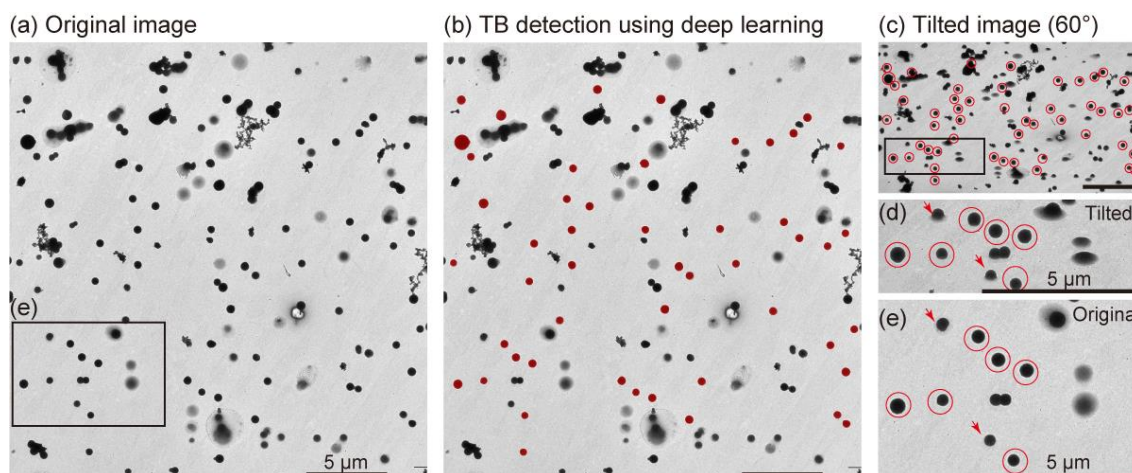
Figure 1. TB detections from TEM images using the deep learning method. (a) The original TEM image. This sample was collected from the Castle fire (14 August, 00:37 UTC). (b) TB detection using the deep learning method. Detected TBs are shown in red. (c) The tilted image of the same area as the original image. The sample was tilted at 60° using a tomography TEM holder. The detected TBs are marked using red circles. (d) The magnified tilted image of the selected area in (c). (e) The magnified image of the selected area in (a). Images (d) and (e) show the same area. Other organic particles spread over the substrates, whereas TBs retain their sphericity. Round particles deformed on the substrate are excluded from the TBs in the deep learning method (red arrows in (d) and (e)). All scale bars indicate 5 µm.

First, 49 TEM images with relatively abundant TB particles from different samples during the FIREX-AQ campaign were selected as teaching images. These TEM images contained 2534 TB particles that were manually identified using conventional imaging techniques (i.e., extraction of spherical particles with high contrast (Adachi et al., 2019)). We constructed a TB model in the software using these TB images and applied the model to the TEM images containing particles used for STEM-EDS analyses (553 images). Then, we extracted particles larger than 0.15 µm, with roundness >0.95 and roughness < 1.05. Finally, the extracted particles were marked as TB in the corresponding particles measured in the STEM-EDS analysis. As a result, we obtained 4567 TB particles with compositional information. All detected TBs were manually checked using TEM images with marked TBs (Figs 1a and 1b) to confirm the image processes. Note that some TBs may be overlooked, especially the coagulated and slightly deformed ones (e.g., Figs. 1d and 1e) because our TB definition is relatively strict compared with conventional imaging analysis. We used this definition to unambiguously select TBs to obtain their averaged compositions and sizes. Thus, the estimated TB number fraction is likely to be lower than that defined by conventional imaging analysis based solely on their spherical shape. We manually checked the presence of aggregated TBs only for the aggregation measurements in Section 3.1.

In addition to the image analysis used for TB identification, we classified all particles into six categories based on their composition. The classification criteria are the same as those in Adachi et al. (2022a): 1) ash-bearing particles (Mg, Ca > 0.5 wt%), 2) mineral dust-bearing particles (Al, Fe > 0.5 wt%), 3) K-bearing particles (K > 2 wt%), 4) sulfate-bearing particles (S > 2 wt%), 5) carbonaceous particles without major inclusions (C + O > 90 wt%), and 6) others (none of the above). When particles were mixtures of two or more particle types (e.g., mineral dust mixed with sulfate), they were classified into a single category as shown in a flow chart (Fig. S1).

We classified all as having attributes of up to seven classes by combining the image analysis (TB identification, primary category) and compositional classification (secondary category): 1) TBs, 2) ash-bearing particles, 3) mineral dust-bearing particles, 4) K-bearing particles, 5) sulfate-bearing particles, 6) carbonaceous particles, and 7) others (Fig. S1). In this

study, the term "carbonaceous particle" is chemically defined and excludes TBs, although TBs are carbonaceous particles. The term "organic particles" is structurally defined based on their amorphous nature in TEM images. The term "other organic particles" refers to organic particles other than TBs.

2.6 Estimation of the tarball mass concentrations and enhancement ratios

205 In addition to the TB number fractions, atmospheric TB mass concentration (TB_{mc}, µg m^{-3}) and TB enhancement ratios relative to carbon monoxide (TB_{mc}/dCO) (i.e., TB_{mc} divided by dCO (ppb), which is $CO_{measured} - CO_{background}$) are useful for evaluating the TB climate effects (Yokelson et al., 2013). Although we did not directly measure atmospheric TB concentrations, we evaluated these values based on our measurements (TB volume fraction) with assumptions such as aerosol densities and particle volumes. Although the estimated values include significant uncertainties originating from, for example,

210 particle collection efficiency (e.g., bouncing effects (Bateman et al., 2017) and loss of volatile particles) and particle viscosity, the attempt will provide an idea of how much TB particles are emitted from biomass burning smoke and the changes that occur with aging.

First, individual aerosol particle volumes are determined based on particle sizes from TEM measurements. We assumed that the TB area-equivalent diameters are the same as the volume-equivalent diameters. Conversely, non-TB particles

215 were highly deformed on the substrates, and an assumption is needed to estimate their volume-equivalent diameters. Cheng et al. (2023) showed a method for estimating particle volume from tilted images and particle aspect ratio. Although we obtained tilted TEM images using a high-tilt tomography TEM holder for selected samples (Fig. 1), the holder cannot be used for the STEM-EDS analysis, and thus the tilted images were not available for most TEM samples. Instead, we assumed that the area-equivalent diameters of non-TB particles became two times larger than their volume-equivalent diameters (Zhang et al., 2020).

220 Second, the densities (g/cm^3) of TB, ash-bearing particles, dust-bearing particles, K-bearing particles, sulfate-bearing particles, carbonaceous particles, and other particles are assumed to be 1.40 (Alexander et al., 2008), 2.70 (as calcium carbonate) (Adachi et al., 2022a), 2.70 (Salcedo et al., 2006), 2.66 (as potassium sulfate) (Patnaik, 2003), 1.75 (Salcedo et al., 2006), 1.20 (Salcedo et al., 2006), and 2.00, respectively. We assume that each particle comprises a single component. Finally, the TB mass fractions estimated from the TEM measurements were applied to the atmospheric aerosol masses obtained by an aerosol mass

225 spectrometer (AMS) to evaluate the TB_{mc} by assuming that the TB volume fractions estimated from our TEM measurements represent those in the sampled air. We used the dataset of the Aerodyne high-resolution time-of-flight aerosol mass spectrometer (HR-ToF-AMS) shown in Adachi et al. (2022a). The AMS had a 50% cutoff size of approximately 870 nm in aerodynamic diameter for typical FIREX-AQ smoke, larger than that of the TEM sampler (~700 nm) (Adachi et al., 2022a). A comparison between TEM measurements and AMS results has been discussed by Adachi et al. (2022a), showing reasonable

230 agreement with uncertainties (e.g., ~50% in sulfate mass). CO mixing ratios in dry air mole fraction were measured by an off-axis integrated cavity output spectrometer (Eilerman et al., 2016; Warneke et al., 2023). Background CO concentrations were estimated from the CO concentrations of air without (or with minimal) biomass burning influences during the campaign.

3 Results and discussion

During the FIREX-AQ campaign, we collected samples from five large wildfires with a wide range of ages (Fig. S2

235 and Table 1). TBs were found in all measured wildfires and agricultural smoke. We show the TB morphology, mixing states, compositions, sizes, and abundances in Section 3.1 and the TB abundance and compositions from different smoke ages in Section 3.2. TBs in a PyroCb event are provided in section 3.3. We discuss the possible TB formation processes in Section 3.4 and the possible implications of our results for climate impacts in Section 3.5.

3.1 Occurrence of tarballs

240 **3.1.1 Morphology and mixing states of the tarballs and other organic particles**

TBs retain the spherical shape with minimal deformation on the substrate. Their spherical shapes indicate that they had solidified in the atmosphere or had a high enough viscosity to retain their sphericity on the substrate, even after being sampled by jet stream impaction. Note that TBs may experience slight deformation on substrates; however, they generally exhibit their maximum diameter near their center with minimal deformations on the contact surface with the substrate (Fig. 1).

245 Most TBs have negligible coatings, i.e., no apparent materials around the TBs, except for those collected in clouds (interstitial samples) (Fig. 2c–d). These spherical TB shapes and negligible coatings are consistent with those found in other samples from various biomass burnings (Pósfai et al., 2004; Hand et al., 2005; Adachi et al., 2019; Yuan et al., 2020), although we found exceptions, as shown in Section 3.3.
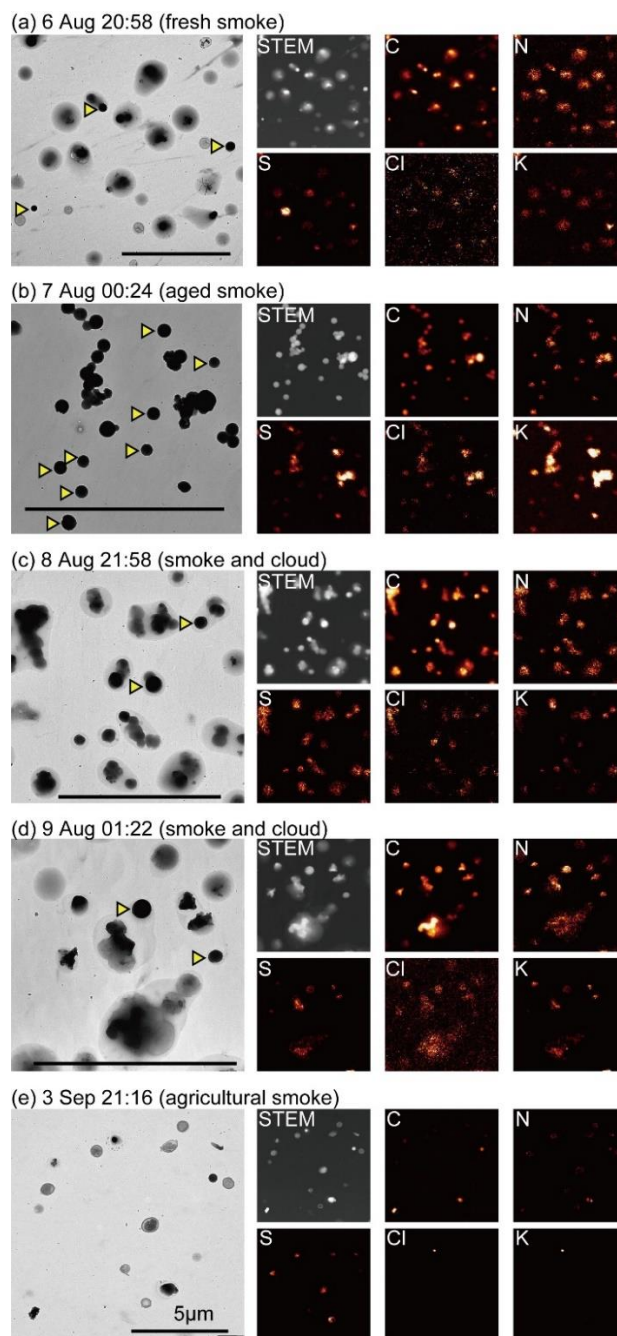
250 **Figure 2. Mapping images of various TEM samples. (a) Fresh (~0.2 h from the emission) and (b) aged (~3.6 h from the emission) samples from the Horsefly wildfire. (c) Wildfire sample within the cloud. (d) Williams Flats wildfire sample within PyroCb. (e) Agricultural smoke sample. Triangles indicate TBs. Scale bars indicate 5 μm.**

Unlike TBs, other organic particles extensively deform on substrates due to their low viscosity, resulting in flattened or dome-shaped configurations (Fig. 1d). Such flattened shapes can be distinguished by a short electron beam path through the thinner particles, which appear brighter than TBs in the TEM image and can also be recognized in the tilted images of representative samples (Fig. 1).

TBs are typically observed as individual particles without mixing or coagulation with other aerosol particles (Pósfai et al., 2004). However, in some cases, TBs may occur in clusters or coagulation forms (Chakrabarty et al., 2006; Girotto et al., 2018). Our samples with relatively high TB number fractions showed TB coagulation (Fig. S3). Approximately 50% of samples with a TB number fraction between 5% and 10% exhibited one or more aggregated TBs in the representative TEM images (Fig. S3). These proportions increased in samples with higher TB number fractions; more than 80% of samples with TB number fractions >25% included aggregated TBs (Fig. S3). Most aggregated TBs comprise several or more primary TBs. In some samples, aggregated TBs comprised tens of TBs (Fig. 3a), although the number of primary TBs is typically lower than that for soot particles, which can contain hundreds of primary particles (Buseck et al., 2014). Although the precise TB aggregation mechanism remains unclear, we hypothesize that TB aggregates form when 1) TB remains solid or highly viscous enough to maintain its spherical shape upon colliding in the atmosphere and 2) the TB concentration is sufficiently high to cause coagulation between particles. By measuring a wide range of biomass burning samples, we found that TBs were also occasionally mixed with other particles such as soot (Fig. 3b), ash particles containing Ca and Mg (Adachi et al., 2022a) (Fig. 3c), and, infrequently, brochosomes derived from leafhoppers (Fig. 3d) (Wittmaack, 2005; Adachi and Buseck, 2013).
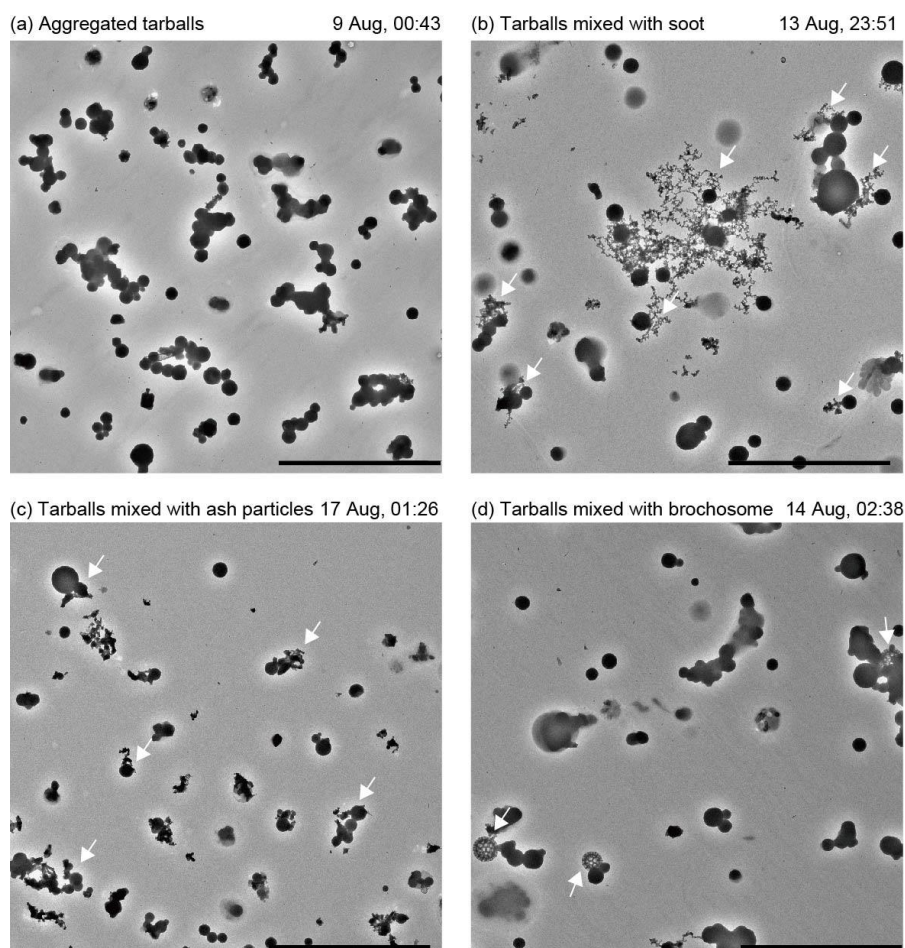
Figure 3. TEM images of coagulated TBs. (a) Aggregated TBs from the Williams Flats fire. (b) TBs coagulated with soot particles from the Castle fire. Arrows indicate soot particles mixed with TBs. (c) TBs coagulated with ash particles from the Sheridan wildfire. Arrows indicate ash particles mixed with TBs. (d) TBs coagulated with brochosomes from the Castle wildfire. Arrows indicate brochosomes. Scale bars indicate 5 μm.

3.1.2 Tarball compositions

TBs consist mainly of carbon (89 ± 4 wt% on average) and oxygen (8 ± 2 wt%). Minor constituents include nitrogen, silicon, sulfur, and potassium (>0.1 wt%), as well as trace amounts of chlorine and iron (>0.05 wt%). These elements detected in TBs are consistent with those reported in previous studies (Pósfai et al., 2004; Hand et al., 2005; Adachi and Buseck, 2011; Chen et al., 2017; Adachi et al., 2019; Yuan et al., 2020). It is possible that TB precursors are primary carbonaceous materials with low viscosity and are inhomogeneously and homogeneously mixed with inorganic compounds (Mathai et al., 2023), including KCl, K_2SO_4, silicon, and nitrate during the TB formation in the smoke.

3.1.3 Tarball sizes

The modal sizes of TBs and carbonaceous particles (non-TBs) in the current study were 0.38 ± 0.08 and 0.49 ± 0.18 μm in area-equivalent diameters, respectively (Fig. 4), which were within the range measured by on-line instruments during the FIREX-AQ campaign (Moore et al., 2021). TBs had smaller and narrower size distributions than carbonaceous particles. One reason why carbonaceous particles exhibit a wider size distribution is their deformation on the substrate, which depends on their viscosity and increases their apparent sizes, as represented by the area-equivalent diameters. In contrast, TBs deform less on the substrate and tend to have geometric sizes similar to those in the atmosphere. It should be noted that some TBs are not perfectly spherical and are slightly elongated when viewed from tilted images, i.e., an average of the aspect ratio of representative TBs in Fig. 1 is ~1.16 from views in the 60-degree tilted TEM images toward the horizontal axis. Thus, their size in the atmosphere before sampling could be slightly smaller than that shown in the current study.

The size of TBs in the FIREX-AQ samples was relatively large compared to that found in previous studies, which showed that TBs typically range between 0.2 and 0.3 μm (Pósfai et al., 2004; Hand et al., 2005; China et al., 2013; Girotto et al., 2018; Adachi et al., 2019; Yoshizue et al., 2020; Yuan et al., 2020), although some studies have also reported larger TBs, measuring over 0.4 μm (Chakrabarty et al., 2006; Tivanski et al., 2007; Fu et al., 2012). Although we could not identify the specific reasons, possible reasons for the large TB sizes in the current study may include differences in the formation processes, such as fuels, burning conditions, and aging, as well as differences in the sampling and measurement conditions.
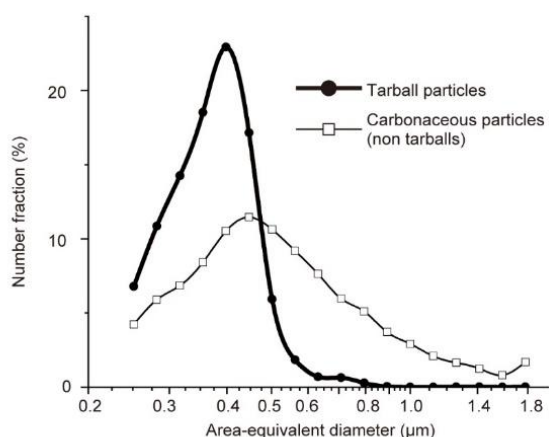
Figure 4. Size distributions of TBs and non-TB carbonaceous particles. The particle size distribution peaks of TB and carbonaceous particles using the Gaussian fit with one sigma value are 0.38 ± 0.08 μm and 0.49±0.18 μm, respectively. Bin sizes are shown in log scale: <0.28, 0.28–0.32, 0.32–0.35, 0.35–0.40, 0.40–0.45, 0.45–0.50, 0.50–0.56, 0.56–0.63, 0.63–0.71, 0.71–0.79, 0.79–0.89, 0.89–1.00, 1.00–1.12, 1.12–1.26, 1.26–1.41, 1.41–1.58, 1.58–1.78, and >1.78 μm. These sizes are all area-equivalent diameters measured from STEM images. n = 4567 and 27307 for TBs and the carbonaceous particles, respectively.

3.1.4 Tarball abundance for each smoke

The TB number fractions for each flight varied between 1% and 20% (10% ± 1% on average with a 95% confidence interval) (Fig. 5). The estimated TB mass fractions for each flight were between 1% and 25% with an average value of 10% ± 2%. The estimated TB_{mc} (µg m^{-3}) and TB enhancement ratios (TB_{mc}/dCO) also varied depending on flights ranging from 2 to 35 µg m^{-3} (10.1 ± 4.6 µg m^{-3} on average) and from 0.001 to 0.03 (0.01 ± 0.002 on average), respectively (see section 2.6 for the method to obtain the mass concentration and the enhancement ratio). The TB abundances and enhancement ratios from the same wildfires, but on different sampling days, were similar (e.g., Williams, Castle, and Sheridan Fires), indicating that the type of wildfire and its fuel sources largely influence the TB emission. In addition, the TB abundance differs significantly depending on the age of the sampled smoke, which is discussed in Section 3.2.
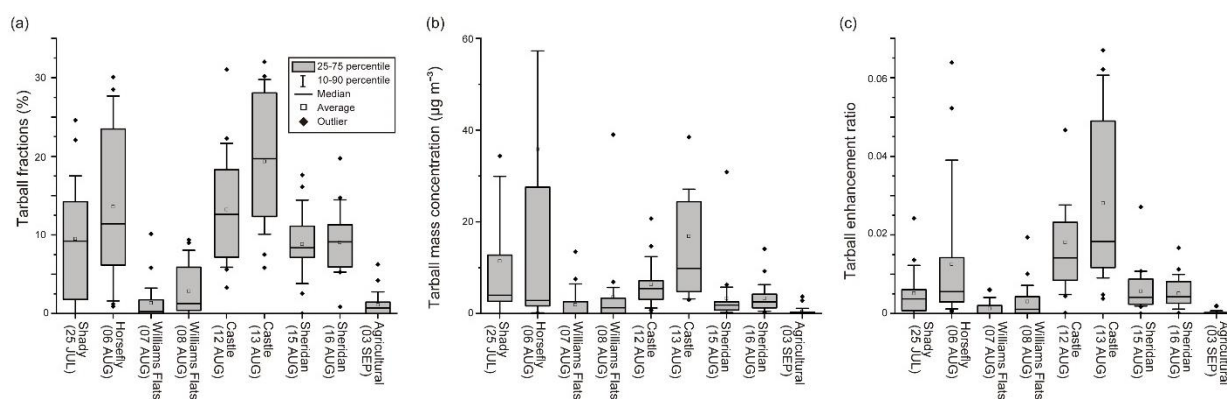
Figure 5. Number fractions, mass concentrations, and enhancement ratios (TB_{mc}/dCO) of the TBs within the TEM samples for each flight.

Agricultural fires emit fewer TBs than wildfires. The TB number fraction, TB_{mc}, and enhancement ratio are 1% ± 1%, 0.5 ± 0.4 µg m^{-3}, and 0.002 ± 0.001, respectively. A possible explanation is differences in their fuel compositions, i.e., woody biomass fuels contain more lignin and cellulose than agricultural biofuels (Travis et al., 2023). Additionally, our TEM study during the FIREX-AQ campaign revealed that inorganic matter (sulfate and K-bearing particles) was more prevalent in agricultural fires than in wildfires (Fig. 6). The differences in their dominant fuel types and burning conditions likely contributed to lower emissions of TBs, compared with wildfires.

3.1.5 Tarball number fractions for each size range

The size-dependent number fractions of aerosol particle types are shown for each flight (Fig. 6). The figures are essentially the same as Fig. S8 in Adachi et al. (2022a), with the addition of the TB fractions in this study (highlighted in yellow in Fig. 6). Unlike other types of aerosols widely distributed across all size ranges, TBs are mainly found in the smaller size ranges (0.25–0.50 µm). The TB fractions are ~20% for wildfires within these small size ranges (<0.5 µm) and are the second largest fraction next to the carbonaceous particle fraction at the size ranges.
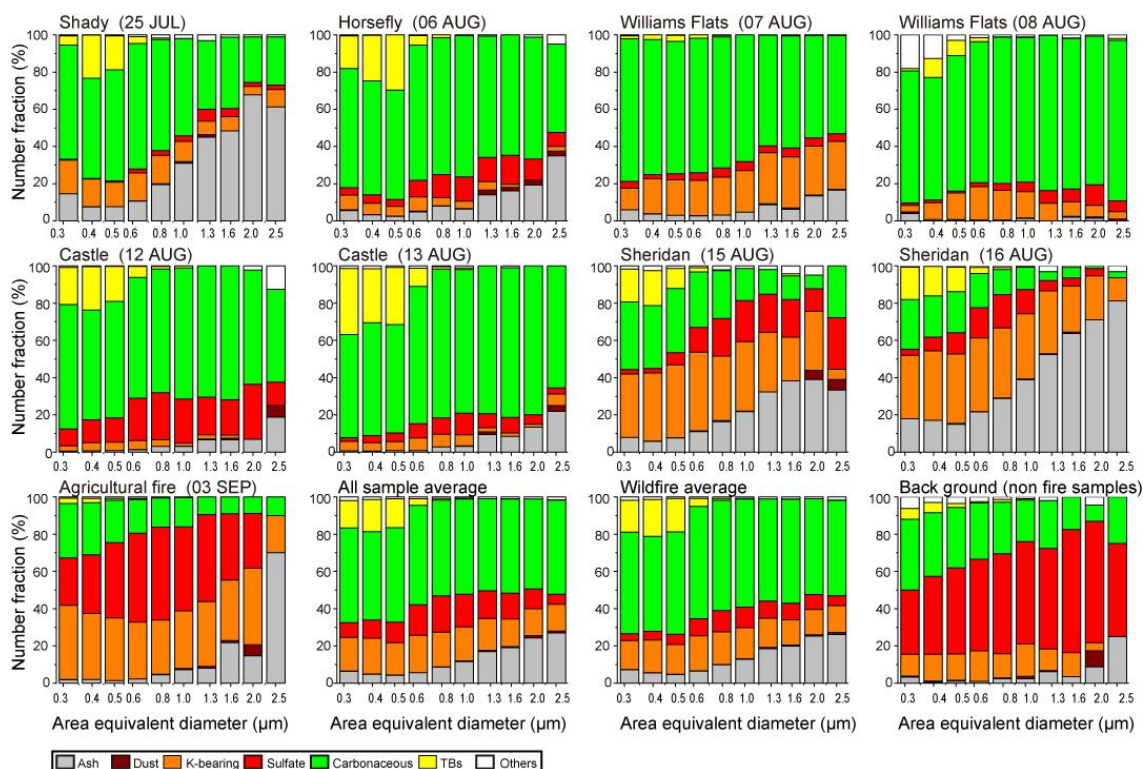
Figure 6. Size-dependent number fractions of aerosol particles collected during the FIREX-AQ campaign. The size bins are 0.25–0.32, 0.32–0.40, 0.40–0.50, 0.50–0.63, 0.63–0.79, 0.79–1.00, 1.00–1.26, 1.26–1.58, 1.58–2.00, and >2.00 μm.

3.2 Tarball abundance and composition in samples with different smoke ages

A series of TEM images demonstrates the TB formation process following an increase in smoke age during the Horsefly fire event on August 6th (Fig. 7). When the samples were collected from the fresh smoke (0.2 h), other organic particles with low viscosity dominated. They spread over the substrate and showed weak contrast in the TEM image (Fig. 7a). Some contained inclusions of either inorganic or organic matter. Some TBs with relatively small sizes were also observed (TB number fraction: 7%). The percentage of TB fractions slightly increased to 11% when samples were taken from smoke that had aged for 1.3 h. However, the sample still contained numerous low-viscosity organic matter (Fig. 7b). As the aging process continued (~2 h), the TB fraction increased to 18% and 23%, resulting in higher apparent organic viscosity with darker contrast in the TEM image (Fig. 7c–d). The most aged samples (>3 h) had a higher number of TBs (29%) and high-viscosity organic matter (Fig. 7f). These aged samples also contained aggregated TBs.
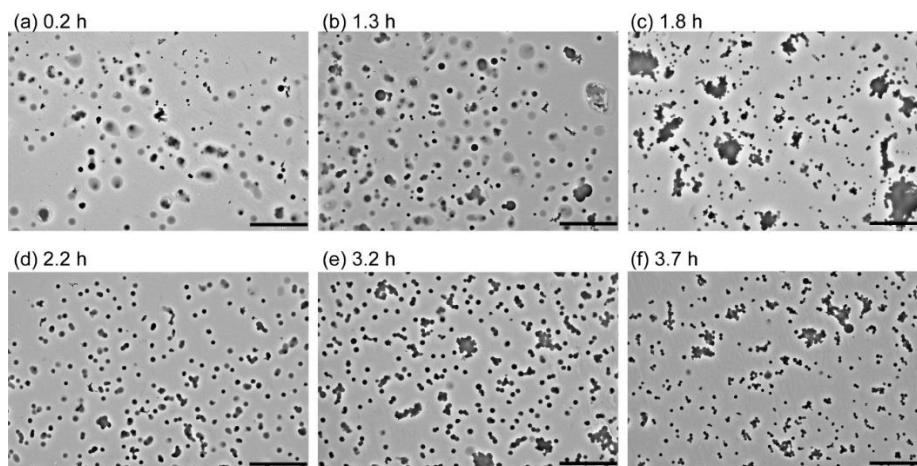
Figure 7. TEM images with different aging and TB fractions in the Horsefly wildfire. Samples were collected on (a) 6 Aug (20:58), (b) 6 Aug (21:19), (c) 6 Aug (23:27), (d) 6 Aug (23:37), (e) 7 Aug (00:11), and (f) 7 Aug (00:22) in UTC. The estimated aging hours (h) from the emissions are shown in each TEM image. The TB number fractions of the corresponding samples were 7%, 11%, 18%, 23%, 24%, and 29%, respectively. Detected TBs are shown in Fig. S4. Scale bars indicate 5 μm.

TB number fractions are plotted along with their estimated smoke age (hours from emission) to compare TB formation in various types of smoke as a function of smoke aging (Fig. 8). Although these plots show large variability, they showed positive correlations for samples younger than ~5 h from the emissions. In particular, the samples from the Horsefly (Fig. 8b) and Williams Flat (Figs. 8c and 8d) fires showed reasonable correlations between TB fractions and the smoke age (R^2 = 0.38, 0.38, and 0.47, respectively). In all samples with the same smoke age, averaged TB number fractions increased from 5% to 15% as the aging proceeded up to 5 h, followed by a subsequent decrease in TB fraction (Fig. 9a). For reference, the TB_{mc} and enhancement ratios at different smoke age are also shown in Fig. 9b and 9c. These values also support the increasing trend up to 5 h from the emissions and the subsequent decreases in the aged smoke (> 5 h). We interpret the results that TB formation was almost complete around 5 h after the emissions. In smoke aged >5 h, the TB abundances started to decrease, likely due to mixing with other aerosol particles from non-biomass burning sources, dilution, and TB removal from the atmosphere, which could mainly contribute to the decrease in TB number fractions, mass concentrations, and enhancement ratios, respectively.
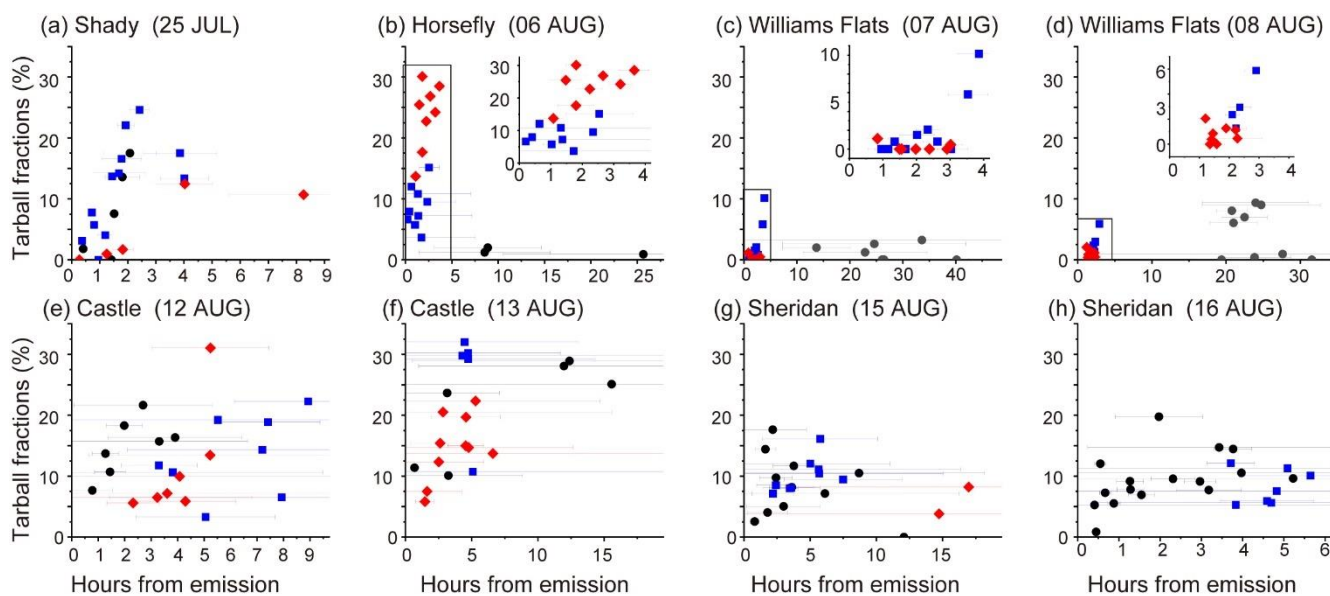
Figure 8. TB number fractions and hours from the emissions for each wildfire (a-h). Different symbols (red diamonds, blue squares, and black circles) in each panel indicate different repeated transect flight patterns for each wildfire smoke (Warneke et al., 2023). Correlation coefficient values (R^2) from (a) to (h) are 0.15, 0.38*, 0.38*, 0.47*, 0.07, 0.26*, 0.06, and 0.04, respectively (*significance level, $p < 0.05$). The R^2 values for (b), (c), and (d) were obtained from two repeated transect flights of less than 4 h, as shown in the upper right of each panel.
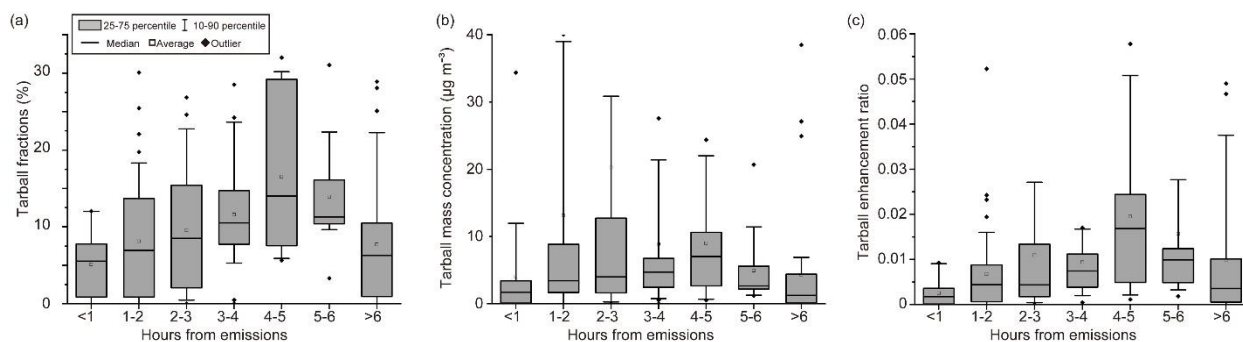
Figure 9. Hourly averaged (a) number fractions, (b) mass concentration (TB$_{mc}$), and (c) enhancement ratios (TB$_{mc}$/dCO) of TB within all wildfire smoke samples. n = 18, 41, 29, 25, 14, 13, and 34 from <1 h to >6 h bins, respectively.

As they aged for up to 6 h, non-sulfate N increased in both TBs and other organic particles (Figs. 10a and 10b). Non-sulfate O in TBs slightly increased with age up to 6 h, but its increase was less clear than that of N (Fig. 10c). Samples from smoke aged <1 h have a high average O concentration (~7 wt%) with large 25–75 percentile ranges because there are only three samples, resulting in a large uncertainty. As they aged, no obvious increase in O was observed in carbonaceous particles (Fig. 10d).

The results of increasing N in TBs as smoke age increases are consistent with those in BBOP (Adachi et al., 2019). It was hypothesized that the increase in organic matter viscosity during TB formation in biomass burning smoke proceeds by the addition of N and O in initially low-viscosity organic particles by the formation of, for example, carboxylic acid and organic nitrogen compounds within several hours of emission by measuring their individual particle compositions using electron energy loss spectrometry and scanning transmission X-ray spectroscopy (Adachi et al., 2019). The current results support this hypothesis for N by analyzing samples that are more aged than those in BBOP (Kleinman et al., 2020). The increase in O with increasing smoke age was not explicitly observed in the current study, and further observations are needed to confirm contributions of O to the TB formation. Increases in N and O in TBs can both decrease (bleaching by oxidation) and increase (formation of organic nitrate) light absorption (Li et al., 2019).
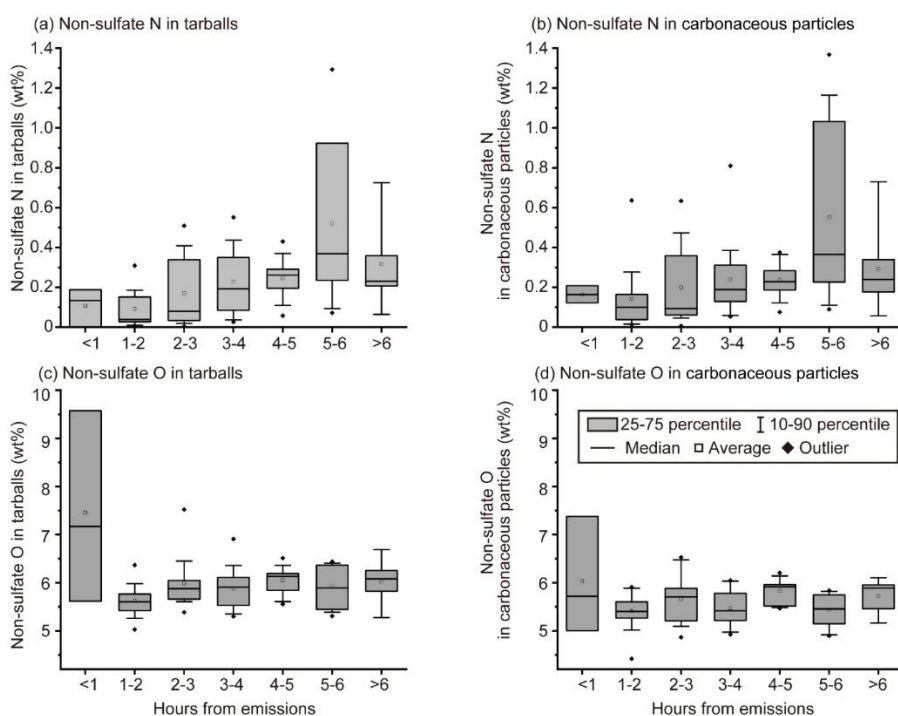
Figure 10. Averaged nitrogen and oxygen weight percent within TBs and carbonaceous particles (non-TBs). Non-sulfate N wt% are shown in (a) TBs and (b) carbonaceous particles. Non-sulfate O wt% are shown in (c) TBs and (d) carbonaceous particles. These plots used averaged values only for the samples having TB number fraction >10% as the samples with few TBs could include background air with well-aged TBs. n = 3, 13, 12, 14, 10, 11, and 9 from <1 h to >6 h bins, respectively.

3.3 Tarballs in pyrocumulonimbus (PyroCb)

During the FIREX-AQ campaign, we had a chance to observe a pyrocumulonimbus (PyroCb) event, which is a thunderstorm that forms from biomass-burning smoke (Peterson et al., 2022; Warneke et al., 2023). The PyroCb occurred in the Williams Flats wildfire smoke that ascended to an altitude of approximately 10 km, which is the upper troposphere and lower stratosphere, and formed ice-phase clouds or mixed-phase clouds of water droplets and ice crystals (Peterson et al., 2022).

The average TB fractions in the Williams Flats smoke were relatively small (1%–3%; Fig. 5 and Table 1) and showed an increase in TB fractions as smoke age increased, similar to other biomass burning smoke (Fig. 8). Representative TEM images of the Williams Flats smoke samples also showed that the viscosity of organic particles was low in the fresh samples (Fig. 11e and 11f) and that the fractions of high-viscosity organic particles increased in the aged samples (Fig. 11a and 11b). The samples collected at the top of PyroCb (~9 km) were dominated by other organic particles with low viscosity and had a small number of TBs (<2% in number fractions) (Fig. 11c and 11d). In the aged samples (Fig. 11a and 11b), a large fraction of high-viscosity organic particles appeared dark and nonspherical in the TEM images.

Some TBs and other organic particles collected in clouds (i.e., interstitial aerosol particles) in the Williams Flats TEM samples had thin layers or coatings (e.g., Figs. 2c, 2d, 11c, and 11d). Such coatings are traces of water mixed with water-soluble matter (Semeniuk et al., 2006) that contain, for example, N, S, and Cl (Fig. 2). Despite water evaporation after sampling, residuals may still surround the water-insoluble cores on the substrate. In the atmosphere, while the smoke ascends, the temperature decreases, and TBs and other aerosol particles can become CCNs and even INPs depending on the temperature, relative humidity, and properties of the aerosol particles (Petters et al., 2009; Jahl et al., 2021). As a result, water condensation or ice development occurred on the particle surface. Nonetheless, some TBs did not show any trace of water-soluble matter, indicating that they were relatively less hygroscopic than other particles (e.g., Fig. 11d). Although ice crystals may have been present in the PyroCb at the sampling altitude (~9 km), they are typically larger than our cutoff sizes (Peterson et al., 2022), making it less probable that the collected particles contained ice crystals.

TBs with a trace of water-soluble matter retained their spherical shapes (Fig. 2d). These results suggest that although some TBs became CCN, they do not comprise highly hygroscopic substances and do not readily dissolve in water or change their shape at a high relative humidity condition (Cheng et al., 2021). This result is inconsistent with that of Hand et al. (2005), who showed the hygroscopic properties of TBs, but agrees with Semeniuk et al. (2006) and Adachi and Buseck (2011), who showed less hygroscopicity of TBs when they were exposed to high relative humidity in the environmental TEM chamber. In conclusion, our observation suggests that TBs can serve as CCNs but exhibit low efficiency.
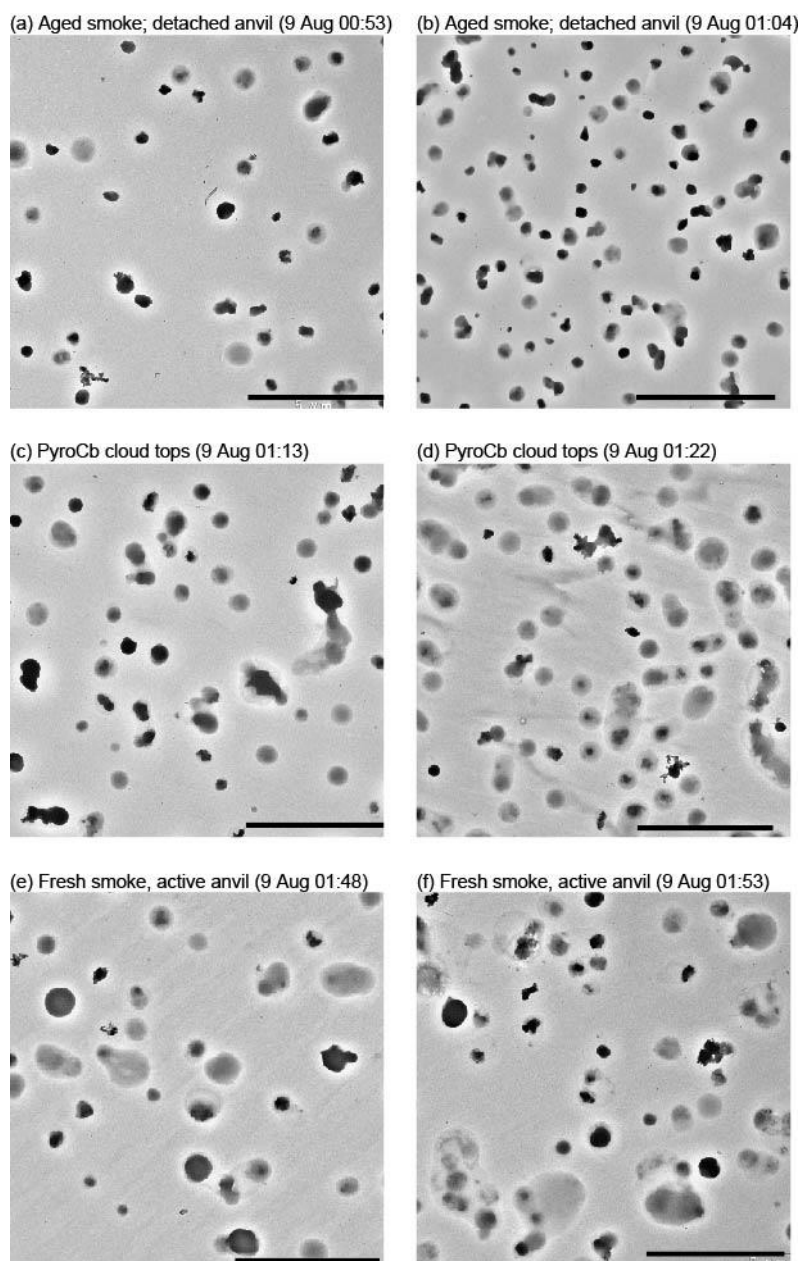
Figure 11. TEM images of aerosol particles within PyroCb from the Williams Flats wildfire. These samples were collected from the same flight with different agings and cloud positions. The sample altitudes were between 7 and 9 km. These samples correspond to transect numbers 1 (a), 2 (b), 4 (c), 5 (d), 8 (e), and 9 (f) in Fig. 4 by Peterson et al. (2022), and the cloud descriptions are also followed by their study. Scale bars indicate 5 μm.

3.4 TB formation

Previous studies have shown TB formation in wildfire smoke, but they focused on moderately aged (up to 3 h) smoke samples (Sedlacek et al., 2018; Adachi et al., 2019). This study showed a similar processed primary particle formation as that shown in Sedlacek et al. (2018) with continued TB formation in more aged smoke (~5 h) (Fig. 9). Formation rates and abundance varied depending on the type of biomass burning smoke. Some had an unclear relationship between TB fractions and smoke age (e.g., Sheridan) and contained only a few TBs (e.g., Williams Flats and most agricultural fires) (Fig. 8 and Table 1). These results suggest that other parameters, in addition to aging, such as fuel type and burning conditions, could also largely contribute to TB formation. Increases in N were observed with increasing age up to 6 h for both TBs and carbonaceous particles (Fig. 10), suggesting the formation of organic nitrogen compounds. This process is likely related to TB formation (Adachi et al., 2019) or proceeded concurrently with it. Nonetheless, the primary factor in TB formation is increasing viscosity

with increasing age. In addition to TB formation, the increase in viscosity of organic particles has implications for gas-particle reactions, affecting reaction degree and speed (Liu et al., 2018; Reid et al., 2018). In future studies, the factors that lead to the increasing viscosity of organic matter, such as addition of specific functional groups (Reid et al., 2018) and water loss, should be measured.

3.5 Implications for climate-relevant properties

TBs are known to be light-absorbing carbon (brown carbon) (Chakrabarty et al., 2010; Sedlacek et al., 2018; Mathai et al., 2023). During FIREX-AQ, Chakrabarty et al. (2023) showed that TBs contributed three-quarters of the short visible light absorption and half of the long visible light absorption within samples collected from ground samplings. The evaluated imaginary refractive index k of the TB from Shady fire ranged between 0.06 ± 0.03 and 0.13 ± 0.04 at a wavelength of 550 nm depending on the burning conditions. They also indicated that TBs are water-insoluble, resist daytime photobleaching, and enhance their light absorption with night-time atmospheric processing. As part of our samples were collected from the same wildfire (e.g., Shady), we assume that they could have similar optical properties.

The degrees of attachment or coating on TBs (i.e., mixing states) affect their hygroscopicity, optical properties, and influences on human health. We found that TBs are sometimes coagulated or attached soot particles (Fig. 3b), resulting in changing their light absorption properties (Lack et al., 2012; Adachi and Buseck, 2013; Saleh et al., 2014). However, TBs did not embed or internally mix with soot, implying the lens effects enhancing the soot absorption (Bond et al., 2006) can be ignored. Our TBs frequently showed aggregated shapes (Fig. S3). Their aggregated shapes influence their optical properties, potentially increases their single-scattering albedo by up to 41% at a wavelength of 550 nm compared with individual TBs (Girotto et al., 2018).

Large biomass burning smoke is rapidly transported to the upper troposphere and lower stratosphere due to the heat produced by the wildfire, forming PyroCb (Fromm et al., 2019; Peterson et al., 2022). Such PyroCb injects significant amounts of biomass burning emissions into the upper troposphere and lower stratosphere. Our measurements found that TBs can also be one of the aerosol species in PyroCb transported to the high atmosphere. Such stratospheric aerosol particles suspend for months, affecting the climate (Katich et al., 2023).

Overall, the influence of TBs on climate depends on their abundance, refractive index, mixing states, morphology, and atmospheric lifetime. These factors can have both positive and negative effects. This study revealed that TBs are not simple inert spherical organic particles but have various appearances that need to be considered regarding their climate influences.

4 Summary and conclusion

This study collected multiple biomass burning smoke and a wider range of aging than previous studies and detected 4567 TBs using a deep learning image analysis method. The number fractions, estimated mass concentrations, and enhancement ratio of TBs increased within 5 h following emissions. Our findings provide further evidence regarding the TB formation via increased viscosity of primary organic matter. They can coagulate with soot and ash particles and other TBs, forming TB coagulations. These mixing states could influence their optical properties. Together with other biomass burning emitted aerosol particles, TBs can be transported to the upper troposphere and lower stratosphere through PyroCb and could survive for months, potentially altering solar radiation. Although TBs can condense water under some conditions, they retained their spherical shapes in the droplets, suggesting that they are sparingly soluble in water. Although TBs have been presumed to be spherical particles that do not mix with other particles, this study found a wide range of TB mixing states that need to be considered when evaluating their climate influences.

Data availability

FIREX-AQ data are available at https://www-air.larc.nasa.gov/cgi-bin/ArcView/firexaq. STEM-EDS data for all individual particles and those for the TEM sample average are available at https://doi.org/10.5281/zenodo.10751569.

Author contributions

KA conducted the TEM analysis and data processing. KA, JED, and JMK set up and executed the TEM sampling. CDH estimated the smoke age. HG, PCJ, and JLJ conducted AMS measurements. JP measured CO concentrations. JPS and JC supervised the campaign. KA prepared the manuscript with contributions from all coauthors.

Competing interests

The authors declare that they have no conflict of interest.

Acknowledgments

We acknowledge the science team members, supporting staff, and the pilots and flight staff of the research aircraft for FIREX-AQ (NASA DC8). KA thanks the Environmental Research and Technology Development Fund (JPMEERF20172003, JPMEERF20202003, JPMEERF20215003, and JPMEERF20232001) of the Environmental Restoration and Conservation Agency of Japan, the Global Environmental Research Coordination System from the Ministry of the Environment of Japan (MLIT1753 and MLIT2253), the Arctic Challenge for Sustainability II (ArCS II) (JPMXD1420318865), and the Japan Society for the Promotion of Science (JSPS) KAKENHI program (grant numbers JP16K16188, JP19K21905, JP19H04259, JP23H03531, and JP23K28221) for financial support. HG, PCJ and JLJ acknowledge NASA Grants 80NSSC21K1451 and 80NSSC23K0828. We especially thank Eric Scheuer (deceased May 2022), who collected all TEM samples during the FIREX-AQ campaign.

References

Abatzoglou, J. T., and Williams, A. P.: Impact of anthropogenic climate change on wildfire across western US forests, Proceedings of the National Academy of Sciences of the United States of America, 113, 11770-11775, 10.1073/pnas.1607171113, 2016.

Adachi, K., and Buseck, P. R.: Atmospheric tar balls from biomass burning in Mexico, Journal of Geophysical Research, 116, D05204, 10.1029/2010jd015102, 2011.

Adachi, K., and Buseck, P. R.: Changes of ns-soot mixing states and shapes in an urban area during CalNex, Journal of Geophysical Research: Atmospheres, 118, 3723-3730, 10.1002/jgrd.50321, 2013.

Adachi, K., Moteki, N. Kondo, Y., and Igarashi, Y.: Mixing states of light-absorbing particles measured using a transmission electron microscope and a single-particle soot photometer in Tokyo, Japan, Journal of Geophysical Research: Atmosphere, 121, 9153–9164, 10.1002/ 2016JD025153, 2016.

Adachi, K., Sedlacek, A. J., Kleinman, L., Chand, D., Hubbe, J. M., and Buseck, P. R.: Volume changes upon heating of aerosol particles from biomass burning using transmission electron microscopy, Aerosol Science and Technology, 52, 46-56, 10.1080/02786826.2017.1373181, 2017.

Adachi, K., Sedlacek, A. J., III, Kleinman, L., Springston, S. R., Wang, J., Chand, D., Hubbe, J. M., Shilling, J. E., Onasch, T. B., Kinase, T., Sakata, K., Takahashi, Y., and Buseck, P. R.: Spherical tarball particles form through rapid chemical and

physical changes of organic matter in biomass-burning smoke, Proceedings of the National Academy of Sciences of the United States of America, 116, 19336-19341, 10.1073/pnas.1900129116, 2019.

520 Adachi, K., Oshima, N., Ohata, S., Yoshida, A., Moteki, N., and Koike, M.: Compositions and mixing states of aerosol particles by aircraft observations in the Arctic springtime, 2018, Atmospheric Chemistry and Physics, 21, 3607-3626, 10.5194/acp-21-3607-2021, 2021.

Adachi, K., Dibb, J. E., Scheuer, E., Katich, J. M., Schwarz, J. P., Perring, A. E., Mediavilla, B., Guo, H., Campuzano-Jost, P., Jimenez, J. L., Crawford, J., Soja, A. J., Oshima, N., Kajino, M., Kinase, T., Kleinman, L., Sedlacek, A. J., Yokelson,

525 R. J., and Buseck, P. R.: Fine ash-bearing particles as a major aerosol component in biomass burning smoke, Journal of Geophysical Research: Atmospheres, 127, e2021JD035657, 10.1029/2021jd035657, 2022a.

Adachi, K., Tobo, Y., Koike, M., Freitas, G., Zieger, P., and Krejci, R.: Composition and mixing state of Arctic aerosol and cloud residual particles from long-term single-particle observations at Zeppelin Observatory, Svalbard, Atmospheric Chemistry and Physics, 22, 14421-14439, 10.5194/acp-22-14421-2022, 2022b.

530 Adachi, K., Tobo, Y., Oshima, N., Yoshida, A., Ohata, S., Krejci, R., Massling, A., Skov, H., and Koike, M.: Composition and mixing state of individual aerosol particles from northeast Greenland and Svalbard in the Arctic during spring 2018, Atmospheric Environment, 314, 120083, 10.1016/j.atmosenv.2023.120083, 2023.

Alexander, D. T., Crozier, P. A., and Anderson, J. R.: Brown carbon spheres in East Asian outflow and their optical properties, Science, 321, 833-836, 10.1126/science.1155296, 2008.

535 Andreae, M. O., and Gelencsér, A.: Black carbon or brown carbon?, Atmospheric Chemistry and Physics, 6, 3131-3148, 2006.

Andreae, M. O.: Emission of trace gases and aerosols from biomass burning – an updated assessment, Atmospheric Chemistry and Physics, 19, 8523-8546, 10.5194/acp-19-8523-2019, 2019.

Barry, K. R., Hill, T. C. J., Levin, E. J. T., Twohy, C. H., Moore, K. A., Weller, Z. D., Toohey, D. W., Reeves, M., Campos, T., Geiss, R., Schill, G. P., Fischer, E. V., Kreidenweis, S. M., and DeMott, P. J.: Observations of ice nucleating particles

540 in the free troposphere from western US wildfires, Journal of Geophysical Research: Atmospheres, 126, e2020JD033752, 10.1029/2020jd033752, 2021.

Bateman, A. P., Gong, Z., Harder, T. H., de Sá, S. S., Wang, B., Castillo, P., China, S., Liu, Y., O'Brien, R. E., Palm, B. B., Shiu, H.-W., Cirino, G. G., Thalman, R., Adachi, K., Alexander, M. L., Artaxo, P., Bertram, A. K., Buseck, P. R., Gilles, M. K., Jimenez, J. L., Laskin, A., Manzi, A. O., Sedlacek, A., Souza, R. A. F., Wang, J., Zaveri, R., and Martin, S. T.:

545 Anthropogenic influences on the physical state of submicron particulate matter over a tropical forest, Atmospheric Chemistry and Physics, 17, 1759–1773, 10.5194/acp-17-1759-2017, 2017.

Beeler, P., Kumar, J., Schwarz, J. P., Adachi, K., Fierce, L., Perring, A. E., Katich, J. M., and Chakrabarty, R. K.: Light absorption enhancement by black carbon in a pyrocumulonimbus cloud, Nature Communications, 15, 6243, 10.1038/s41467-024-50070-0, 2024.

550 Bond, T. C., Habib, G., and Bergstrom, R. W.: Limitations in the enhancement of visible light absorption due to mixing state, Journal of Geophysical Research, 111, D20211, 10.1029/2006jd007315, 2006.

Brock, C. A., Williamson, C., Kupc, A., Froyd, K. D., Erdesz, F., Wagner, N., Richardson, M., Schwarz, J. P., Gao, R.-S., Katich, J. M., Campuzano-Jost, P., Nault, B. A., Schroder, J. C., Jimenez, J. L., Weinzierl, B., Dollner, M., Bui, T., and Murphy, D. M.: Aerosol size distributions during the Atmospheric Tomography Mission (ATom): methods, uncertainties,

555 and data products, Atmospheric Measurement Techniques, 12, 3081-3099, 10.5194/amt-12-3081-2019, 2019.

Buseck, P. R., Adachi, K., Gelencsér, A., Tompa, É., and Pósfai, M.: Ns-Soot: A material-based term for strongly light-absorbing carbonaceous particles, Aerosol Science and Technology, 48, 777-788, 10.1080/02786826.2014.919374, 2014.

Chakrabarty, R. K., Moosmüller, H., Garro, M. A., Arnott, W. P., Walker, J., Susott, R. A., Babbitt, R. E., Wold, C. E., Lincoln, E. N., and Hao, W. M.: Emissions from the laboratory combustion of wildland fuels: Particle morphology and size,

560 Journal of Geophysical Research, 111, D07204, 10.1029/2005jd006659, 2006.

Chakrabarty, R. K., Moosmüller, H., Chen, L. W. A., Lewis, K., Arnott, W. P., Mazzoleni, C., Dubey, M. K., Wold, C. E., Hao, W. M., and Kreidenweis, S. M.: Brown carbon in tar balls from smoldering biomass combustion, Atmospheric Chemistry and Physics, 10, 6363-6370, 10.5194/acp-10-6363-2010, 2010.

Chakrabarty, R. K., Shetty, N. J., Thind, A. S., Beeler, P., Sumlin, B. J., Zhang, C., Liu, P., Idrobo, J. C., Adachi, K., Wagner, N. L., Schwarz, J. P., Ahern, A., Sedlacek, A. J., Lambe, A., Daube, C., Lyu, M., Liu, C., Herndon, S., Onasch, T. B., and Mishra, R.: Shortwave absorption by wildfire smoke dominated by dark brown carbon, Nature Geoscience, 16, 683-688, 10.1038/s41561-023-01237-9, 2023.

Chen, J., Li, C., Ristovski, Z., Milic, A., Gu, Y., Islam, M. S., Wang, S., Hao, J., Zhang, H., He, C., Guo, H., Fu, H., Miljevic, B., Morawska, L., Thai, P., Lam, Y. F., Pereira, G., Ding, A., Huang, X., and Dumka, U. C.: A review of biomass burning: Emissions and impacts on air quality, health and climate in China, Science of the Total Environment, 579, 1000-1034, 10.1016/j.scitotenv.2016.11.025, 2017.

Cheng, Z., Sharma, N., Tseng, K. P., Kovarik, L., and China, S.: Direct observation and assessment of phase states of ambient and lab-generated sub-micron particles upon humidification, RSC Adv., 11, 15264–15272, 10.1039/d1ra02530a, 2021.

Cheng, Z., Morgenstern, M., Henning, S., Zhang, B., Roberts, G. C., Fraund, M., Marcus, M. A., Lata, N. N., Fialho, P., Mazzoleni, L., Wehner, B., Mazzoleni, C., and China, S.: Cloud condensation nuclei activity of internally mixed particle populations at a remote marine free troposphere site in the North Atlantic Ocean, Sci. Total Environ., 904, 166865, 10.1016/j.scitotenv.2023.166865, 2023.

China, S., Mazzoleni, C., Gorkowski, K., Aiken, A. C., and Dubey, M. K.: Morphology and mixing state of individual freshly emitted wildfire carbonaceous particles, Nature Communications, 4, 2122, 10.1038/ncomms3122, 2013.

Corbin, J. C., and Gysel-Beer, M.: Detection of tar brown carbon with a single particle soot photometer (SP2), Atmospheric Chemistry and Physics, 19, 15673-15690, 10.5194/acp-19-15673-2019, 2019.

Decker, Z. C. J., Robinson, M. A., Barsanti, K. C., Bourgeois, I., Coggon, M. M., DiGangi, J. P., Diskin, G. S., Flocke, F. M., Franchin, A., Fredrickson, C. D., Gkatzelis, G. I., Hall, S. R., Halliday, H., Holmes, C. D., Huey, L. G., Lee, Y. R., Lindaas, J., Middlebrook, A. M., Montzka, D. D., Moore, R., Neuman, J. A., Nowak, J. B., Palm, B. B., Peischl, J., Piel, F., Rickly, P. S., Rollins, A. W., Ryerson, T. B., Schwantes, R. H., Sekimoto, K., Thornhill, L., Thornton, J. A., Tyndall, G. S., Ullmann, K., Van Rooy, P., Veres, P. R., Warneke, C., Washenfelder, R. A., Weinheimer, A. J., Wiggins, E., Winstead, E., Wisthaler, A., Womack, C., and Brown, S. S.: Nighttime and daytime dark oxidation chemistry in wildfire plumes: an observation and model analysis of FIREX-AQ aircraft data, Atmospheric Chemistry and Physics, 21, 16293-16317, 10.5194/acp-21-16293-2021, 2021.

Eilerman, S. J., Peischl, J., Neuman, J. A., Ryerson, T. B., Aikin, K. C., Holloway, M. W., Zondlo, M. A., Golston, L. M., Pan, D., Floerchinger, C., and Herndon, S.: Characterization of ammonia, methane, and nitrous oxide emissions from concentrated animal feeding operations in northeastern Colorado, Environmental Science and Technology, 50, 10885–10893, 10.1021/acs.est.6b02851, 2016.

Fromm, M., Peterson, D., and Di Girolamo, L.: The primary convective pathway for observed wildfire emissions in the upper troposphere and lower stratosphere: a targeted reinterpretation, Journal of Geophysical Research: Atmospheres, 124, 13254-13272, 10.1029/2019jd031006, 2019.

Fu, H., Zhang, M., Li, W., Chen, J., Wang, L., Quan, X., and Wang, W.: Morphology, composition and mixing state of individual carbonaceous aerosol in urban Shanghai, Atmospheric Chemistry and Physics, 12, 693-707, 10.5194/acp-12-693-2012, 2012.

Girotto, G., China, S., Bhandari, J., Gorkowski, K., Scarnato, B. V., Capek, T., Marinoni, A., Veghte, D. P., Kulkarni, G., Aiken, A. C., Dubey, M., and Mazzoleni, C.: Fractal-like tar ball aggregates from wildfire smoke, Environmental Science & Technology Letters, 5, 360-365, 10.1021/acs.estlett.8b00229, 2018.

Gkatzelis, G. I., Coggon, M. M., Stockwell, C. E., Hornbrook, R. S., Allen, H., Apel, E. C., Bela, M. M., Blake, D. R., Bourgeois, I., Brown, S. S., Campuzano-Jost, P., St. Clair, J. M., Crawford, J. H., Crounse, J. D., Day, D. A., DiGangi, J. P., Diskin, G. S., Fried, A., Gilman, J. B., Guo, H., Hair, J. W., Halliday, H. S., Hanisco, T. F., Hannun, R., Hills, A., Huey, L. G., Jimenez, J. L., Katich, J. M., Lamplugh, A., Lee, Y. R., Liao, J., Lindaas, J., McKeen, S. A., Mikoviny, T., Nault, B. A., Neuman, J. A., Nowak, J. B., Pagonis, D., Peischl, J., Perring, A. E., Piel, F., Rickly, P. S., Robinson, M. A., Rollins, A. W., Ryerson, T. B., Schueneman, M. K., Schwantes, R. H., Schwarz, J. P., Sekimoto, K., Selimovic, V., Shingler, T., Tanner, D. J., Tomsche, L., Vasquez, K. T., Veres, P. R., Washenfelder, R., Weibring, P., Wennberg, P. O., Wisthaler, A., Wolfe, G. M., Womack, C. C., Xu, L., Ball, K., Yokelson, R. J., and Warneke, C.: Parameterizations of US wildfire and prescribed fire emission ratios and emission factors based on FIREX-AQ aircraft measurements Atmospheric Chemistry and Physics, 24, 929–956, 10.5194/acp-24-929-2024, 2024.

Hand, J. L., Malm, W. C., Laskin, A., Day, D., Lee, T., Wang, C., Carrico, C., Carrillo, J., Cowin, J. P., Collett, J., and Iedema, M. J.: Optical, physical, and chemical properties of tar balls observed during the Yosemite Aerosol Characterization Study, Journal of Geophysical Research, 110, D21210, 10.1029/2004jd005728, 2005.

Hoffer, A., Tóth, A., Nyirő-Kósa, I., Pósfai, M., and Gelencsér, A.: Light absorption properties of laboratory-generated tar ball particles, Atmospheric Chemistry and Physics, 16, 239-246, 10.5194/acp-16-239-2016, 2016.

Jacobson, M. Z.: Investigating cloud absorption effects: Global absorption properties of black carbon, tar balls, and soil dust in clouds and aerosols, Journal of Geophysical Research: Atmospheres, 117, D06205, 10.1029/2011jd017218, 2012.

Jaffe, D. A., O'Neill, S. M., Larkin, N. K., Holder, A. L., Peterson, D. L., Halofsky, J. E., and Rappold, A. G.: Wildfire and prescribed burning impacts on air quality in the United States, Journal of the Air & Waste Management Association, 70, 583-615, 10.1080/10962247.2020.1749731, 2020.

Jahl, L. G., Brubaker, T. A., Polen, M. J., Jahn, L. G., Cain, K. P., Bowers, B. B., Fahy, W. D., Graves, S., and Sullivan, R. C.: Atmospheric aging enhances the ice nucleation ability of biomass-burning aerosol, Science Advances, 7, eabd3440, 10.1126/sciadv.abd3440, 2021.

Junghenn Noyes, K. T., Kahn, R. A., Limbacher, J. A., Li, Z., Fenn, M. A., Giles, D. M., Hair, J. W., Katich, J. M., Moore, R. H., Robinson, C. E., Sanchez, K. J., Shingler, T. J., Thornhill, K. L., Wiggins, E. B., and Winstead, E. L.: Wildfire smoke particle properties and evolution, from space-based multi-angle imaging II: The Williams Flats fire during the FIREX-AQ campaign, Remote Sensing, 12, 3823, 10.3390/rs12223823, 2020.

Karanasiou, A., Alastuey, A., Amato, F., Renzi, M., Stafoggia, M., Tobias, A., Reche, C., Forastiere, F., Gumy, S., Mudu, P., and Querol, X.: Short-term health effects from outdoor exposure to biomass burning emissions: A review, Science of the Total Environment, 781, 146739, 10.1016/j.scitotenv.2021.146739, 2021.

Katich, J. M., Apel, E. C., Bourgeois, I., Brock, C. A., Bui, T. P., Campuzano-Jost, P., Commane, R., Daube, B., Dollner, M., Fromm, M., Froyd, K. D., Hills, A. J., Hornbrook, R. S., Jimenez, J. L., Kupc, A., Lamb, K. D., McKain, K., Moore, F., Murphy, D. M., Nault, B. A., Peischl, J., Perring, A. E., Peterson, D. A., Ray, E. A., Rosenlof, K. H., Ryerson, T., Schill, G. P., Schroder, J. C., Weinzierl, B., Thompson, C., Williamson, C. J., Wofsy, S. C., Yu, P., and Schwarz, J. P.: Pyrocumulonimbus affect average stratospheric aerosol composition, Science, 379, 815-820, 10.1126/science.add3101, 2023.

Keywood, M., Kanakidou, M., Stohl, A., Dentener, F., Grassi, G., Meyer, C. P., Torseth, K., Edwards, D., Thompson, A. M., Lohmann, U., and Burrows, J.: Fire in the air: biomass burning impacts in a changing climate, Critical Reviews in Environmental Science and Technology, 43, 40-83, 10.1080/10643389.2011.604248, 2011.

Kleinman, L. I., Sedlacek, A. J., Adachi, K., Buseck, P. R., Collier, S., Dubey, M. K., Hodshire, A. L., Lewis, E., Onasch, T. B., Pierce, J. R., Shilling, J., Springston, S. R., Wang, J., Zhang, Q., Zhou, S., and Yokelson, R. J.: Rapid evolution of aerosol particles and their optical properties downwind of wildfires in the western US, Atmospheric Chemistry and Physics, 20, 13319-13341, 10.5194/acp-20-13319-2020, 2020.

Lack, D. A., Langridge, J. M., Bahreini, R., Cappa, C. D., Middlebrook, A. M., and Schwarz, J. P.: Brown carbon and internal mixing in biomass burning particles, Proceedings of the National Academy of Sciences of the United States of America, 109, 14802-14807, 10.1073/pnas.1206575109, 2012.

Laskin, A., Laskin, J., and Nizkorodov, S. A.: Chemistry of atmospheric brown carbon, Chemical Revews, 115, 4335-4382, 10.1021/cr5006167, 2015.

Li, C., He, Q., Schade, J., Passig, J., Zimmermann, R., Meidan, D., Laskin, A., and Rudich, Y.: Dynamic changes in optical and chemical properties of tar ball aerosols by atmospheric photochemical aging, Atmospheric Chemistry and Physics, 19, 139-163, 10.5194/acp-19-139-2019, 2019.

Li, J., Pósfai, M., Hobbs, P. V., and Buseck, P. R.: Individual aerosol particles from biomass burning in southern Africa: 2, Compositions and aging of inorganic particles, Journal of Geophysical Research: Atmospheres, 108, D13, 8484, 10.1029/2002jd002310, 2003.

Liao, J., Wolfe, G. M., Hannun, R. A., St. Clair, J. M., Hanisco, T. F., Gilman, J. B., Lamplugh, A., Selimovic, V., Diskin, G. S., Nowak, J. B., Halliday, H. S., DiGangi, J. P., Hall, S. R., Ullmann, K., Holmes, C. D., Fite, C. H., Agastra, A., Ryerson, T. B., Peischl, J., Bourgeois, I., Warneke, C., Coggon, M. M., Gkatzelis, G. I., Sekimoto, K., Fried, A., Richter, D., Weibring, P., Apel, E. C., Hornbrook, R. S., Brown, S. S., Womack, C. C., Robinson, M. A., Washenfelder, R. A., Veres, P. R., and Neuman, J. A.: Formaldehyde evolution in US wildfire plumes during the Fire Influence on Regional to Global Environments and Air Quality experiment (FIREX-AQ), Atmospheric Chemistry and Physics, 21, 18319-18331, 10.5194/acp-21-18319-2021, 2021.

Liu, P., Li, Y. J., Wang, Y., Bateman, A. P., Zhang, Y., Gong, Z., Bertram, A. K., and Martin, S. T.: Highly viscous states affect the browning of atmospheric organic particulate matter, ACS Central Science, 4, 207-215, 10.1021/acscentsci.7b00452, 2018.

Mathai, S., Veghte, D., Kovarik, L., Mazzoleni, C., Tseng, K., Bucci, S., Capek, T., Cheng, Z., Marinoni, A., and China, S.: Optical Properties of Individual Tar Balls in the Free Troposphere, Environ. Sci. Technol., 57, 16834–16842, 10.1021/acs.est.3c03498, 2023.

McNaughton, C. S., Clarke, A. D., Howell, S. G., Pinkerton, M., Anderson, B., Thornhill, L., Hudgins, C., Winstead, E., Dibb, J. E., Scheuer, E., and Maring, H.: Results from the DC-8 Inlet Characterization Experiment (DICE): Airborne Versus Surface Sampling of Mineral Dust and Sea Salt Aerosols, Aerosol Science and Technology, 41, 136-159, 10.1080/02786820601118406, 2007.

Moore, R. H., Wiggins, E. B., Ahern, A. T., Zimmerman, S., Montgomery, L., Campuzano Jost, P., Robinson, C. E., Ziemba, L. D., Winstead, E. L., Anderson, B. E., Brock, C. A., Brown, M. D., Chen, G., Crosbie, E. C., Guo, H., Jimenez, J. L., Jordan, C. E., Lyu, M., Nault, B. A., Rothfuss, N. E., Sanchez, K. J., Schueneman, M., Shingler, T. J., Shook, M. A., Thornhill, K. L., Wagner, N. L., and Wang, J.: Sizing response of the Ultra-High Sensitivity Aerosol Spectrometer (UHSAS) and Laser Aerosol Spectrometer (LAS) to changes in submicron aerosol composition and refractive index, Atmospheric Measurement Techniques, 14, 4517-4542, 10.5194/amt-14-4517-2021, 2021.

Moroni, B., Cappelletti, D., Crocchianti, S., Becagli, S., Caiazzo, L., Traversi, R., Udisti, R., Mazzola, M., Markowicz, K., Ritter, C., and Zielinski, T.: Morphochemical characteristics and mixing state of long range transported wildfire particles at Ny-Ålesund (Svalbard Islands), Atmospheric Environment, 156, 135-145, 10.1016/j.atmosenv.2017.02.037, 2017.

Moroni, B., Ritter, C., Crocchianti, S., Markowicz, K., Mazzola, M., Becagli, S., Traversi, R., Krejci, R., Tunved, P., and Cappelletti, D.: Individual particle characteristics, optical properties and evolution of an extreme long-range transported biomass burning event in the European Arctic (Ny-Ålesund, Svalbard Islands), Journal of Geophysical Research: Atmospheres, 125, e2019JD031535, 10.1029/2019jd031535, 2020.

Pagonis, D., Selimovic, V., Campuzano-Jost, P., Guo, H., Day, D. A., Schueneman, M. K., Nault, B. A., Coggon, M. M., DiGangi, J. P., Diskin, G. S., Fortner, E. C., Gargulinski, E. M., Gkatzelis, G. I., Hair, J. W., Herndon, S. C., Holmes, C.

D., Katich, J. M., Nowak, J. B., Perring, A. E., Saide, P., Shingler, T. J., Soja, A. J., Thapa, L. H., Warneke, C., Wiggins,
690   E. B., Wisthaler, A., Yacovitch, T. I., Yokelson, R. J., and Jimenez, J. L.: Impact of biomass burning organic aerosol
        volatility on smoke concentrations downwind of fires, Environmental Science and Technology, 57, 17011-17021,
        10.1021/acs.est.3c05017, 2023.

Pardo, M., Li, C., He, Q., Levin-Zaidman, S., Tsoory, M., Yu, Q., Wang, X., and Rudich, Y.: Mechanisms of lung toxicity
        induced by biomass burning aerosols, Particle and Fibre Toxicology, 17, 4, 10.1186/s12989-020-0337-x, 2020.

695   Patnaik, P.: Handbook of Inorganic Chemicals, McGraw-Hill, New York, 2003.

Peterson, D. A., Thapa, L. H., Saide, P. E., Soja, A. J., Gargulinski, E. M., Hyer, E. J., Weinzierl, B., Dollner, M., Schöberl,
        M., Papin, P. P., Kondragunta, S., Camacho, C. P., Ichoku, C., Moore, R. H., Hair, J. W., Crawford, J. H., Dennison, P.
        E., Kalashnikova, O. V., Bennese, C. E., Bui, T. P., DiGangi, J. P., Diskin, G. S., Fenn, M. A., Halliday, H. S., Jimenez,
        J., Nowak, J. B., Robinson, C., Sanchez, K., Shingler, T. J., Thornhill, L., Wiggins, E. B., Winstead, E., and Xu, C.:
700   Measurements from inside a Thunderstorm Driven by Wildfire: The 2019 FIREX-AQ Field Experiment, Bulletin of the
        American Meteorological Society, E2140–E2167, 10.1175/bams-d-21-0049.1, 2022.

Petters, M. D., Carrico, C. M., Kreidenweis, S. M., Prenni, A. J., DeMott, P. J., Collett, J. L., and Moosmüller, H.: Cloud
        condensation nucleation activity of biomass burning aerosol, Journal of Geophysical Research, 114, D22205,
        10.1029/2009jd012353, 2009.

705   Pósfai, M., Simonics, R., Li, J., Hobbs, P. V., and Buseck, P. R.: Individual aerosol particles from biomass burning in southern
        Africa: 1. Compositions and size distributions of carbonaceous particles, Journal of Geophysical Research: Atmospheres,
        108, 8483, 10.1029/2002jd002291, 2003.

Pósfai, M., Gelencsér, A., Simonics, R., Arató, K., Li, J., Hobbs, P. V., and Buseck, P. R.: Atmospheric tar balls: Particles
        from biomass and biofuel burning, Journal of Geophysical Research: Atmospheres, 109, D06213, 10.1029/2003jd004169,
710   2004.

Reid, J. P., Bertram, A. K., Topping, D. O., Laskin, A., Martin, S. T., Petters, M. D., Pope, F. D., and Rovelli, G.: The viscosity
        of atmospherically relevant organic particles, Nature Communications, 9, 956, 10.1038/s41467-018-03027-z, 2018.

Saleh, R., Robinson, E. S., Tkacik, D. S., Ahern, A. T., Liu, S., Aiken, A. C., Sullivan, R. C., Presto, A. A., Dubey, M. K.,
        Yokelson, R. J., Donahue, N. M., and Robinson, A. L.: Brownness of organics in aerosols from biomass burning linked
715   to their black carbon content, Nature Geoscience, 7, 647-650, 10.1038/ngeo2220, 2014.

Salcedo, D., Onasch, T. B., Dzepina, K., Canagaratna, M. R., Zhang, Q., Huffman, J. A., DeCarlo, P. F., Jayne, J. T., Mortimer,
        P., Worsnop, D. R., Kolb, C. E., Johnson, K. S., Zuberi, B., Marr, L. C., Volkamer, R., Molina, L. T., Molina, M. J.,
        Cardenas, B., Bernabé, R. M., Márquez, C., Gaffney, J. S., Marley, N. A., Laskin, A., Shutthanandan, V., Xie, Y., Brune,
        W., Lesher, R., Shirley, T., and Jimenez, J. L.: Characterization of ambient aerosols in Mexico City during the MCMA-
720   2003 campaign with Aerosol Mass Spectrometry: results from the CENICA Supersite, Atmospheric Chemistry and
        Physics, 6, 925–946, 10.5194/acp-6-925-2006, 2006.

Sedlacek, A. J., Buseck, P. R., Adachi, K., Onasch, T. B., Springston, S. R., and Kleinman, L.: Formation and evolution of tar
        balls from northwestern US wildfires, Atmospheric Chemistry and Physics, 18, 11289-11301, 10.5194/acp-18-11289-
        2018, 2018.

725   Semeniuk, T. A., Wise, M. E., Martin, S. T., Russell, L. M., and Buseck, P. R.: Hygroscopic behavior of aerosol particles from
        biomass fires using environmental transmission electron microscopy, Journal of Atmospheric Chemistry, 56, 259-273,
        10.1007/s10874-006-9055-5, 2006.

Siemens, K. S. A., Pagonis, D., Guo, H., Schueneman, M. K., Dibb, J. E., Campuzano-Jost, P., Jimenez, J. L., and Laskin, A.:
        Probing atmospheric aerosols by multimodal mass spectrometry techniques: Revealing aging characteristics of its
730   individual molecular components, ACS Earth and Space Chemistry, 7, 2498-2510, 10.1021/acsearthspacechem.3c00228,
        2023.

Sparks, T. L., and Wagner, J.: Composition of particulate matter during a wildfire smoke episode in an urban area, Aerosol Science and Technology, 55, 734-747, 10.1080/02786826.2021.1895429, 2021.

Stein, A. F., Draxler, R. R., Rolph, G. D., Stunder, B. J. B., Cohen, M. D., and Ngan, F.: NOAA's HYSPLIT atmospheric transport and dispersion modeling system, Bulletin of the American Meteorological Society, 96, 2059-2077, 10.1175/bams-d-14-00110.1, 2015.

Sumlin, B., Fortner, E., Lambe, A., Shetty, N. J., Daube, C., Liu, P., Majluf, F., Herndon, S., and Chakrabarty, R. K.: Diel cycle impacts on the chemical and light absorption properties of organic carbon aerosol from wildfires in the western United States, Atmospheric Chemistry and Physics, 21, 11843-11856, 10.5194/acp-21-11843-2021, 2021.

Szopa, S., Naik, V., Adhikary, B., Artaxo, P., Berntsen, T., Collins, W. D., Fuzzi, S., Gallardo, L., Kiendler-Scharr, A., Klimont, Z., Liao, H., Unger, N., and Zanis, P.: Short-lived climate forcers., in: Climate Change 2021: The physical science basis. Contribution of working group I to the sixth assessment report of the Intergovernmental Panel on Climate Change, edited by: Masson-Delmotte, V., Zhai, P., Pirani, A., Connors, S. L., Péan, C., Berger, S., Caud, N., Chen, Y., Goldfarb, L., Gomis, M. I., Huang, M., Leitzell, K., Lonnoy, E., Matthews, J. B. R., Maycock, T. K., Waterfield, T., Yelekçi, O., Yu, R., and Zhou, B., Cambridge University Press, Cambridge, , United Kingdom and New York, NY, USA, 817–922, 2021.

Tivanski, A. V., Hopkins, R. J., Tyliszczak, T., and Gilles, M. K.: Oxygenated interface on biomass burn tar balls determined by single particle scanning transmission X-ray microscopy, The Journal of Physical Chemistry A, 111, 5448-5458, 10.1021/jp070155u, 2007.

Tóth, A., Hoffer, A., Nyirő-Kósa, I., Pósfai, M., and Gelencsér, A.: Atmospheric tar balls: aged primary droplets from biomass burning?, Atmospheric Chemistry and Physics, 14, 6669-6675, 10.5194/acp-14-6669-2014, 2014.

Travis, K. R., Crawford, J. H., Soja, A. J., Gargulinski, E. M., Moore, R. H., Wiggins, E. B., Diskin, G. S., DiGangi, J. P., Nowak, J. B., Halliday, H., Yokelson, R. J., McCarty, J. L., Simpson, I. J., Blake, D. R., Meinardi, S., Hornbrook, R. S., Apel, E. C., Hills, A. J., Warneke, C., Coggon, M. M., Rollins, A. W., Gilman, J. B., Womack, C. C., Robinson, M. A., Katich, J. M., Peischl, J., Gkatzelis, G. I., Bourgeois, I., Rickly, P. S., Lamplugh, A., Dibb, J. E., Jimenez, J. L., Campuzano-Jost, P., Day, D. A., Guo, H., Pagonis, D., Wennberg, P. O., Crounse, J. D., Xu, L., Hanisco, T. F., Wolfe, G. M., Liao, J., St. Clair, J. M., Nault, B. A., Fried, A., and Perring, A. E.: Emission factors for crop residue and prescribed fires in the eastern US during FIREX-AQ, Journal of Geophysical Research: Atmospheres, 128, e2023JD039309, 10.1029/2023jd039309, 2023.

Warneke, C., Schwarz, J. P., Dibb, J., Kalashnikova, O., Frost, G., Al-Saad, J., Brown, S. S., Brewer, W. A., Soja, A., Seidel, F. C., Washenfelder, R. A., Wiggins, E. B., Moore, R. H., Anderson, B. E., Jordan, C., Yacovitch, T. I., Herndon, S. C., Liu, S., Kuwayama, T., Jaffe, D., Johnston, N., Selimovic, V., Yokelson, R., Giles, D. M., Holben, B. N., Goloub, P., Popovici, I., Trainer, M., Kumar, A., Pierce, R. B., Fahey, D., Roberts, J., Gargulinski, E. M., Peterson, D. A., Ye, X., Thapa, L. H., Saide, P. E., Fite, C. H., Holmes, C. D., Wang, S., Coggon, M. M., Decker, Z. C. J., Stockwell, C. E., Xu, L., Gkatzelis, G., Aikin, K., Lefer, B., Kaspari, J., Griffin, D., Zeng, L., Weber, R., Hastings, M., Chai, J., Wolfe, G. M., Hanisco, T. F., Liao, J., Campuzano Jost, P., Guo, H., Jimenez, J. L., and Crawford, J.: Fire influence on regional to global environments and air quality (FIREX-AQ), Journal of Geophysical Research: Atmospheres, 128, e2022JD037758, 10.1029/2022jd037758, 2023.

Wittmaack, K.: Brochosomes produced by leafhoppers-a widely unknown, yet highly abundant species of bioaerosols in ambient air, Atmospheric Environment, 39, 1173-1180, 10.1016/j.atmosenv.2004.11.003, 2005.

Xu, L., Crounse, J. D., Vasquez, K. T., Allen, H., Wennberg, P. O., Bourgeois, I., Brown, S. S., Campuzano-Jost, P., Coggon, M. M., Crawford, J. H., DiGangi, J. P., Diskin, G. S., Fried, A., Gargulinski, E. M., Gilman, J. B., Gkatzelis, G. I., Guo, H., Hair, J. W., Hall, S. R., Halliday, H. A., Hanisco, T. F., Hannun, R. A., Holmes, C. D., Huey, L. G., Jimenez, J. L., Lamplugh, A., Lee, Y. R., Liao, J., Lindaas, J., Neuman, J. A., Nowak, J. B., Peischl, J., Peterson, D. A., Piel, F., Richter, D., Rickly, P. S., Robinson, M. A., Rollins, A. W., Ryerson, T. B., Sekimoto, K., Selimovic, V., Shingler, T., Soja, A. J.,

775   St. Clair, J. M., Tanner, D. J., Ullmann, K., Veres, P. R., Walega, J., Warneke, C., Washenfelder, R. A., Weibring, P., Wisthaler, A., Wolfe, G. M., Womack, C. C., and Yokelson, R. J.: Ozone chemistry in western U.S. wildfire plumes, Science Advances, 7, eabl3648, 10.1126/sciadv.abl3648, 2021.

Yokelson, R. J., Urbanski, S. P., Atlas, E. L., Toohey, D. W., Alvarado, E. C., Crounse, J. D., Wennberg, P. O., Fisher, M. E., Wold, C. E., Campos, T. L., Adachi, K., Buseck, P. R., and Hao, W. M.: Emissions from forest fires near Mexico City,

780   Atmospheric Chemistry and Physics, 7, 5569-5584, 10.5194/acp-7-5569-2007, 2007.

Yokelson, R. J., Andreae, M. O., and Akagi, S. K.: Pitfalls with the use of enhancement ratios or normalized excess mixing ratios measured in plumes to characterize pollution sources and aging, Atmospheric Measurement Techniques, 6, 2155–2158, 10.5194/amt-6-2155-2013, 2013.

Yoshizue, M., Taketani, F., Adachi, K., Iwamoto, Y., Tohjima, Y., Mori, T., and Miura, K.: Detection of aerosol particles from

785   Siberian biomass burning over the western north Pacific, Atmosphere, 11, 10.3390/atmos11111175, 2020.

Yuan, Q., Xu, J., Liu, L., Zhang, A., Liu, Y., Zhang, J., Wan, X., Li, M., Qin, K., Cong, Z., Wang, Y., Kang, S., Shi, Z., Pósfai, M., and Li, W.: Evidence for large amounts of brown carbonaceous tarballs in the Himalayan atmosphere, Environmental Science & Technology Letters, 8, 16-23, 10.1021/acs.estlett.0c00735, 2020.

Zeng, L., Dibb, J., Scheuer, E., Katich, J. M., Schwarz, J. P., Bourgeois, I., Peischl, J., Ryerson, T., Warneke, C., Perring, A.

790   E., Diskin, G. S., DiGangi, J. P., Nowak, J. B., Moore, R. H., Wiggins, E. B., Pagonis, D., Guo, H., Campuzano-Jost, P., Jimenez, J. L., Xu, L., and Weber, R. J.: Characteristics and evolution of brown carbon in western United States wildfires, Atmospheric Chemistry and Physics, 22, 8009-8036, 10.5194/acp-22-8009-2022, 2022.

Zhang, J., Liu, L., Xu, L., Lin, Q., Zhao, H., Wang, Z., Guo, S., Hu, M., Liu, D., Shi, Z., Huang, D., and Li, W.: Exploring wintertime regional haze in northeast China: role of coal and biomass burning, Atmospheric Chemistry and Physics, 20,

795   5355-5372, 10.5194/acp-20-5355-2020, 2020.